30641

National Library of Canada
Bibliothèque nationale du Canada

CANADIAN THESES ON MICROFICHE
THÈSES CANADIENNES SUR MICROFICHE

NAME OF AUTHOR/*NOM DE L'AUTEUR* CHEE, KIM TOON

TITLE OF THESIS/*TITRE DE LA THÈSE* SINGLE AND DOUBLE INJECTION CUPROUS OXIDE DIODES.

UNIVERSITY/*UNIVERSITÉ* Univ of Alberta.

DEGREE FOR WHICH THESIS WAS PRESENTED/ *GRADE POUR LEQUEL CETTE THÈSE FUT PRÉSENTÉE* Ph. D.

YEAR THIS DEGREE CONFERRED/*ANNÉE D'OBTENTION DE CE GRADE* Fall, 1976

NAME OF SUPERVISOR/*NOM DU DIRECTEUR DE THÈSE* DR. F. L. WEICHMAN.

Permission is hereby granted to the NATIONAL LIBRARY OF CANADA to microfilm this thesis and to lend or sell copies of the film.

The author reserves other publication rights, and neither the thesis nor extensive extracts from it may be printed or otherwise reproduced without the author's written permission.

L'autorisation est, par la présente, accordée à la BIBLIOTHÈQUE NATIONALE DU CANADA de microfilmer cette thèse et de prêter ou de vendre des exemplaires du film.

L'auteur se réserve les autres droits de publication; ni la thèse ni de longs extraits de celle-ci ne doivent être imprimés ou autrement reproduits sans l'autorisation écrite de l'auteur.

DATED/*DATÉ* Nov. 1 1976 SIGNED/*SIGNÉ* Chee

PERMANENT ADDRESS/*RÉSIDENCE FIXE*
11045 - 89 Ave.
Edmonton Alberta

NL-91 (3-74)

INFORMATION TO USERS

THIS DISSERTATION HAS BEEN
MICROFILMED EXACTLY AS RECEIVED

This copy was produced from a microfiche copy of the original document. The quality of the copy is heavily dependent upon the quality of the original thesis submitted for microfilming. Every effort has been made to ensure the highest quality of reproduction possible.

PLEASE NOTE: Some pages may have indistinct print. Filmed as received.

Canadian Theses Division
Cataloguing Branch
National Library of Canada
Ottawa, Canada K1A 0N4

AVIS AUX USAGERS

LA THESE A ETE MICROFILMEE
TELLE QUE NOUS L'AVONS RECUE

Cette copie a été faite à partir d'une microfiche du document original. La qualité de la copie dépend grandement de la qualité de la thèse soumise pour le microfilmage. Nous avons tout fait pour assurer une qualité supérieure de reproduction.

NOTA BENE: La qualité d'impression de certaines pages peut laisser à désirer. Microfilmee telle que nous l'avons reçue.

Division des thèses canadiennes
Direction du catalogage
Bibliothèque nationale du Canada
Ottawa, Canada K1A 0N4

THE UNIVERSITY OF ALBERTA

SINGLE AND DOUBLE INJECTION
CUPROUS OXIDE DIODES

by

© CHEE, KIM TOON

A THESIS

SUBMITTED TO THE FACULTY OF GRADUATE STUDIES AND RESEARCH
IN PARTIAL FULFILMENT OF THE REQUIREMENTS FOR THE DEGREE
OF DOCTOR OF PHILOSOPHY

DEPARTMENT OF PHYSICS

EDMONTON, ALBERTA

FALL, 1976

THE UNIVERSITY OF ALBERTA

FACULTY OF GRADUATE STUDIES AND RESEARCH

The undersigned certify that they have read, and recommend to the Faculty of Graduate Studies and Research, a thesis entitled Single and Double Injection Cuprous Oxide Diodes, submitted by Chee Kim Toon in partial fulfilment of the requirements for the degree of Doctor of Philosophy.

Frank L. Weichman
Supervisor

External Examiner

Date Oct. 18 1976

ABSTRACT

The unsatisfactory performance of conventional multicrystalline Cu_2O rectifiers, particularly in the reversed bias condition, triggered us to attempt to make Cu_2O single crystal rectifiers. The method of fabricating these rectifiers is reported. The study of these rectifiers supported a previous suggestion that grain boundaries are responsible for one of the deteriorations observed in conventional Cu_2O rectifiers.

We also found the I-V characteristics of the diodes we made are very different from conventional Cu_2O diodes whose characteristics are controlled by the Cu_2O-Cu junction.

We have studied the forward current-voltage characteristics of the single-crystal rectifiers in great detail. Two sets of diodes, one annealed under high vacuum (10^{-6} torr) and the other at higher air pressure (1-2 torr), were studied. They show the characteristics of injection diodes.

Since conduction due to single or double carrier injection has not previously been reported for Cu_2O, a detailed study of the characteristics of these Cu_2O diodes was made and the results were compared with the theory of single or double injection.

We found the vacuum-annealed samples show characteristics which agree with the theory of single-carrier space-charge-limited conduction . From the I-V characteristics of the samples and other experimental results, we conclude that there is a continuous distribution of localized states inside the energy band gap for this type of sample preparation.

On the other hand, the diodes which were annealed at higher air pressure were found to exhibit the characteristics of double injection. The low injection regimes were studied in detail. For thick samples, the experimental results were found to agree well with the simplified theory of double injection. However, discrepancies were observed for thinner samples. Preliminary results on negative resistance observed in these diodes at higher injection level are also reported.

ACKNOWLEDGEMENT

It is a great pleasure to thank Dr. F.L. Weichman for suggesting the research project and also his patient help and encouragement during the entire course of this work.

I would also like to thank Mr. G. Christie for his technical assistance during all stages of the work.

The teaching assistantship provided by the Department of Physics and the Izaak Walton Killam Memorial Scholarship awarded by the Killam Scholarship Committee are also gratefully acknowledged.

K.T.C.

Table of Contents

Chapter | Page

1. Introduction 1

2. Fabrication of Cu_2O single-crystal Diodes and Techniques of Measurement 4

3. Pt-Cu_2O-Cu Structure as a Diode 25

4. Pt-Cu_2O-Cu Single Injection Diodes 37

5. Pt-Cu_2O-Cu Double Injection Diodes 79

6. Conclusion 129

Bibliography 131

Appendix A: List of Symbols 134

Appendix B: Recombination Through a Set of Localized States 138

LIST OF FIGURES

Figure		Page
1.	The Forward Conductance of Cu_2O Single Crystal Diodes (Sample SD-3) versus the Time of Exposure to Air	12
2a.	A View of the Structure of the Cu_2O Single Crystal Diode	14
2b.	Cross Section View of the Cu_2O Single Crystal Diode	14
2c.	A Simplified Diagram of the Electrical Circuit Used for I-V Measurement	15
3.	Diagram Showing the Current Components for Guard Ring Arrangement	16
4.	A Diagramatic View of the Vacuum Pumping System	19
5a.	Sample Chamber	20
5b.	Cross Section of the Sample Holder	21
5c.	Top View of the Sample Holder	21
6.	The Forward Conductance of the Cu_2O Single Crystal Diode (Sample SD-3) versus the Reciprocal of the Absolute Temperature	23
7.	The Current-Voltage Characteristic of Sample S-9 Before Oxidation	27
8.	The Current-Voltage Characteristic of Sample S-9 After Oxidation	28
9.	The Reversed Current versus the Duration of Reversed Voltage	31
10.	The Reversed Current at 30 Volts versus Elapsed Time	33
11.	The Effect of Heating at 130°C in Air on the Current-Voltage Characteristics of Cu_2O Single-Crystal Diodes	35

Figure Page

12. Schematic Energy-Band Diagram of a p-type Semiconductor under Forward Bias Condition 41

13. Schematic Energy-Band Diagram of a Semiconductor with Shallow Traps at Energy E_t 46

14. Schematic Energy-Band Diagram of a Semiconductor with a Distribution of Traps Following an Exponential Decrease in Density with Energy 48

15. The Activation Energies of Cu_2O Crystals verses Their Corresponding Resistivity at 20°C. (After Zielinger et. al. 1972) 53

16. The Forward I-V Characteristics of Vacuum-Annealed Sample SD-10 at a Temperature of 270°K 57

17. The Forward I-V Characteristics of Vacuum-Annealed Sample SD-10 at Various Temperatures. 60

18. The Forward Conductance of Sample SD-10 versus the Reciprocal of Absolute Temperature 62

19. The Current at 300 Volts Versus the Thickness of the Cu_2O Single Crystal (Vacuum-Annealed Sample) 66

20. Dark Current versus Time of Light Exposure (Photomemory Effect) 69

21. The Forward I-V Characteristics of Vacuum-Annealed Sample SD-10 at Temperature 273°K 72

22. The Transient Current Response to a Voltage Step 75

23. Transient Current for Single-Carrier SCL Diode in Response to a Voltage Step, with Trap Present 77

Figure Page

24. Schematic Energy-Band Diagram for a Semiconductor, With Partially Filled Recombination Centers, at Thermal Equilibrium 84

25. The Forward I-V Characteristics of Oxidized Sample SD-1 at Various Temperatures 97

26. The Forward I-V Characteristics of Oxidized Sample SD-2 at Room Temperature 99

27. The Forward I-V Characteristics of Oxidized Sample SD-2 at Various Temperatures 101

28. The Currents in the Ohmic Regime and the $I\alpha V^{3/2}$ Regime versus the Reciptocal of Absolute Temperature (Sample SD-1) 104

29. The Forward Current-Voltage Characteristic of Oxidized Sample SD-2 at Room Temperature 107

30. Log_{10} $(J_{3/2}/J_1)$ versus $\mathrm{Log}_{10}L$, where $J_{3/2}$ is the current at 10 volts ($I\alpha V^{3/2}$ Regime), J_1 the Current at 0.1 Volts (Ohmic Regime) and L the Thickness in μm. (Sample SD-6) 111

31. Schematic Diagram for Lampert's Regional Approximation Applied to the Case of Double Injection with Trapping by Partially Filled Recombination Centers 114

32. Current-Voltage Characteristic for Double Injection into an Insulator with a Single Set of Recombination Centers Partially Filled in Thermal Equilibrium. (Theoretical Calculation, After Lampert and Mark, 1970) 118

33. A Qualitative Sketch of the Current-Voltage Characteristic to be Expected for Double Injection into an Insulator with a Single Set of Recombination Centers Partially filled in Thermal Equilibrium, Including the Lower-Level Injection Regimes 119

Figure Page

34. Oscillograms of the Current-Voltage Characteristics of Oxidized Sample SD-4 at 178°K 123

35. Oscillograms of the I-V Characteristics of Oxidized Sample SD-4 at (a) 185°K and (b) 183°K 125

36. Oscillogram of the I-V Characteristic of Oxidized Sample SD-4 at 236°K 127

Chapter 1

Introduction

Conventional cuprous oxide (Cu_2O) rectifiers were among the first rectifiers in use in the early twenties (Grondahl 1926). However, its behaviour, especially under reversed biased condition, has long been known to exhibit undesirable effects such as the increase of reversed current with respect to time after preparation of the rectifiers. It was suggested that the boundaries between the microcrystalline Cu_2O grain grown on the copper was responsible for some of this deterioration. A natural step to take was then to prepare single crystal rectifiers. As conventional methods of obtaining rectifiers by oxidizing copper sheet are always found to be multicrystalline (with the exception of certain facets when single crystal copper is used), we have attempted to make Cu_2O single crystal rectifiers starting from Cu_2O single crystals. This method of preparing these diodes is described in chapter 2.

The study of these Cu_2O single-crystal diodes indicates that although some deterioration can be removed by using single crystals, other undesirable effects under the reversed biased condition still exist in these diodes (chapter 3). During this study, the rather interesting behaviour of the forward current-voltage characteristics was noticed. Work has since then been focused on the investigation of these characteristics.

It was found that the behaviour of these diodes depended on the annealing process the diodes received after their preparation. Various experiments indicate these diodes are injection diodes, that is, the I-V characteristics observed are due to the injection of excess carriers from the electrodes into the crystals. For the first time in Cu_2O, various injection regimes are observed in the I-V characteristics which are discussed in detail in chapters 4 and 5.

We found the vacuum-annealed samples show characteristics which agree with the theory of single-carrier space-charge-limited conductions. The I-V characteristics of the samples and other experimental results indicate that there is a continuous distribution of localized states inside the energy band gap.

On the other hand, the diodes which were annealed at higher air pressure were found to exhibit the characteristics of double injection. The low injection regimes were studied in detail. For thick samples, the experimental results were found to agree well with the simplified theory of double injection. However, discrepancies were observed for thinner samples. Preliminary results on negative resistance observed in these diodes at higher injection level are also reported.

In the past, studies on electrical conduction in Cu_2O crystal were almost exclusively in the ohmic regime. Although much valuable information can be obtained from these studies, some interpretations are rather ambiguous. For example, Roberts and Schmidlin (1969) pointed out that the interpretation of the activation energy in the ohmic conduction regime will be ambiguous unless other supplementary observations, such as that of single-carrier space-charge-limited conduction, are included.

The discovery and study of the various injection regimes in single and double injection Cu_2O diodes reported in this thesis therefore serve to widen the scope of research on the conduction regimes in Cu_2O. It is hoped that this study can shed some light on the understanding of Cu_2O, a material which is still not clearly understood even after over half a century of study.

Chapter 2

Fabrication of Cu_2O Single-crystal Diodes and Techniques of Measurement

(1) Motivation for preparing Cu_2O single-crystal diodes:

The making of conventional types of Cu_2O-Cu rectifiers involves the oxidation of copper discs or copper sheets at temperatures over 1000°C followed by an annealing and/or quenching process (Grondahl 1933, Greiner 1961). The CuO layer is then either polished or etched away, leaving the Cu_2O layer on top of the copper. Multicrystalline Cu_2O layers are always obtained using this method. It has been shown in the past that the reversed current of the rectifiers started to deteriorate (increase) immediately after their preparation (Kuzel 1961). Two types of deterioration can be distinguished. One is that the reversed current increases above the tolerable level as time progresses, the second that the reversed current increases with time while a constant voltage is applied. This second effect is usually referred to as the creeping effect.

The first effect was found to be partly due to the formation of a low-resistance layer along the edges of the rectifiers. Etching the edges could in most cases restore the reversed current to its original value.

The creeping effect could be overcome by heating the rectifiers for 10-20 minutes at 100°C - 150°C. Kuzel (1961) showed that this heat treatment increased the stability of the reversed current. However, excess heating (e.g. 1 hour) at this temperature for such rectifiers caused the reversed current to increase. This was explained by the fact that in multicrystalline cuprous oxide rectifiers, the oxygen rich layer between the grains formed barrier layers at the metal - semiconductor boundary, but of much poorer quality than those formed at the bulk semiconductor - metal boundary (Weichman and Kuzel 1970a). Extensive heating at 100°C - 150°C caused the deterioration of these grain boundary layers. It was found that this type of deterioration could take place at room temperature over a period of days rather than hours. A natural step to improve Cu_2O-Cu rectifiers was seen to be the attempt to make single crystal Cu_2O rectifiers and therefore eliminate the undesirable effect due to the grain boundaries.

(2) Method for preparing Cu_2O single-crystal diodes:

Cuprous oxide single crystals, of the order of one square centimeter in area and of thickness 0.5 to 1 mm., are cut from larger Cu_2O slabs which also contain smaller crystals. The slabs are grown from high-purity copper (ASARCO) by the grain growth method (Toth et. al. 1961).

In most crystals, there are voids near the central region of the crystal. This region contains a high degree of imperfections. Crystals are chosen and mounted in such a way that this region is at a sufficient distance from the face that is to be bonded to the copper, so that it can be completely removed by grinding and polishing after the bonding process.

The two larger faces of the crystal are polished flat and approximately parallel to each other on Logitech PM2 polishing machine. During polishing, the sample is attached to a jig (Logitech polishing jig, PP5) by resin or glue. The jig, together with the sample, is lapped against a brass plate with 12.5 micron aluminium oxide powder as an abrasive.

To obtain approximately parallel faces on the single crystal sample, we proceed in three steps. First, one of the faces of the sample is polished flat on the brass plate. Then this crystal is removed from the jig. A second piece of Cu_2O, which we will refer to as the reference piece, is mounted to the jig and also polished flat on the same plate. Without removing this reference piece of Cu_2O from the jig, the polished face of the sample is now placed in contact with the polished face of the reference piece. Acrylic cement is applied on the edge of the sample and a brass weight is placed on the top of the crystal to press it tightly against the reference piece. The weight is removed when the cement is cured (2 hours or more). The exposed side of the sample is then polished. In principle, it is obvious that, since the faces of the sample are parallel to the brass plate, they are parallel to each other. In practice, it is found that, as long as the brass plate is kept in good condition, the degree of parallelism is better than 1 micrometer for a width of 1 centimeter, which is sufficient for our purpose.

After both sides have been polished, the sample is rinsed with acetone, followed by etching a few times (about half a minute each time) with dilute HNO_3 (i.e. 1/4 concentrated HNO_3 in 3/4 water).

To make the actual diode we proceed as follows.

First, we form a thin copper layer on the surface of the Cu_2O. This is done by placing the sample in the dilute HNO_3 to reduce the surface to copper. This copper layer, however, is easily wiped off and care must be taken to avoid this while rinsing the sample in water to remove the remaining HNO_3. The crystal, with its copper layer, is then placed in a horizontal oven subsequently evacuated with a roughing pump and a molecular sieve absorption pump to a pressure of about 10^{-4} torr. The oven is then heated to approximately 600°C and maintained at that temperature for 3 hours, after which the oven is slowly allowed to cool to room temperature. The Cu_2O crystal treated in this way will be found to have a thin coating of copper which adheres well.

A second, larger piece of Cu_2O material, but not normally a single crystal, is similarly prepared to act as a substrate of identical coefficient of expansion as the crystal which is to be bonded to it. The copper-coated Cu_2O crystal is placed on a similarly coated Cu_2O substrate, separate from it by a thin ($\approx$ 50 μm) copper foil. This Cu_2O - Cu - Cu_2O sandwich is again placed in the horizontal oven which is again evacuated. This time the oven is heated to 1020°C and maintained at that temperature for 5 to 10 minutes. The temperature must then be increased to 1100°C to melt the copper foil. After approximately 10 minutes at 1100°C, the heating current is switched off and the oven is allowed to cool to room temperature over a period of 15 hours.

With this procedure the Cu_2O crystal will be found to be well bonded to the copper and, through it, to the Cu_2O substrate.

The Cu_2O single crystal of the sandwich must now be polished thinner, usually to a thickness of the order of 50 to 200 μm. The exposed face of the substrate is polished flat and parallel to the exposed face of the sample using the method described before. The polishing process is now repeated with the exposed face of the sample lapping against the brass plate.

Finally, platinum electrodes are sputtered onto the exposed face of the Cu_2O crystal. Platinum is also sputtered onto the exposed surfaces of the Cu_2O substrate in such a way that contact to the central copper layer can be assured. This allows electrical contact to the copper to be made on the larger platinum surfaces rather than directly to the smaller areas of protruding copper.

This process completes the manufacture of each individual diode. Since, as will be reported in chapter 4, the behaviour of such a diode can be strongly influenced by subsequent annealing treatment, we will describe the final individual treatment where we discuss the experimental results obtained from that diode.

(3) Electrical measurement devices - method and apparatus:

One major source of error in the early literature on the electrical properties of cuprous oxide has been the fact that the surface conductivity of this material very often is appreciably higher than the bulk conductivity. The formation of a highly conducting surface layer occurs when the sample is exposed to air. This layer, however, can be removed by heating to around 160°C or higher in vacuum. Fig. 1 shows an example of this effect. The forward conductance of a diode is plotted against the time of exposure to air. The diode has been preheated to 200°C in vacuum to remove the high conductivity layer. Once the sample is exposed to air at room temperature, the forward conductance measured without a guard ring (curve 1) begins to climb as time progresses, while the measurement with a guard ring (curve 2), as described below, shows no change in forward conductance in response to air exposure. This clearly indicates the formation of the conducting surface layer.

Therefore, when measuring the current-voltage characteristics of diodes, precautions have to be taken to eliminate such surface leakage currents, or to correct for their presence by appropriate measurement techniques.

Two methods have been used by us to obtain true bulk current results:

Fig. 1. The forward conductance of Cu_2O single crystal diodes (sample SD-3) versus the time of exposure to air. The sample has been preheated at about 200°C in vacuum. The data points ○ (curve 1) were taken without guard ring on sample, while data points ● (curve 2) were taken with guard ring on the sample.
(The detail heat treatment of sample SD-3 is identical with that of sample SD-10 described in chapter 4.)

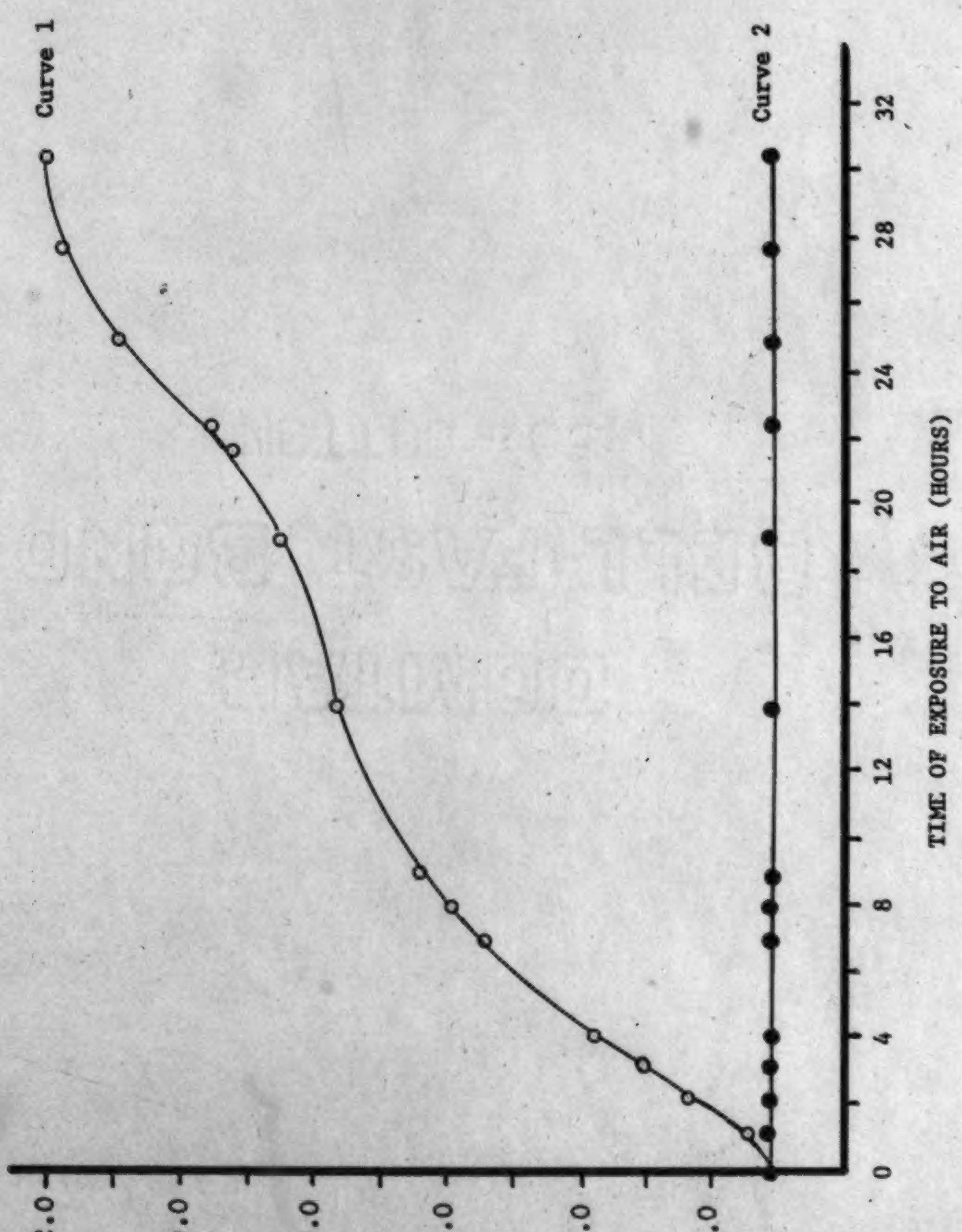
Curve 1
Curve 2
FORWARD CONDUCTANCE (X10^{-8} ohm^{-1})
12.0
10.0
8.0
6.0
4.0
2.0
0
4
8
12
16
20
24
28
32
TIME OF EXPOSURE TO AIR (HOURS)

(i) Guard-ring method: For I-V measurement in air, guard rings are provided (Fig. 2). The internal resistance R of the current measuring device is required to be smaller than the resistance R_s between the guard ring and the central electrode since it is obvious that the surface current I_s between the central electrode and the guard ring should be much smaller than the current I_R through R (refer to Fig. 3), that is,

$$I_s << I_R \quad .$$

since

$$I_s = \frac{I_R R}{R_s} \, ,$$

we have

$$\frac{I_R R}{R_s} << I_R \, ,$$

or

$$R << R_s \quad .$$

This method is very convenient for low resistivity samples. For measurements on high-resistivity samples, where the current measuring device must be far more sensitive and therefore often of higher internal impedance, this method is more difficult to apply.

(ii) Vacuum pre-heating method: This second method involves the elimination of surface current by heating the sample to about 200°C in vacuum (≈ 10^{-6} torr) and cooling to room temperature under vacuum. All subsequent measurements are then made in vacuum or under inert

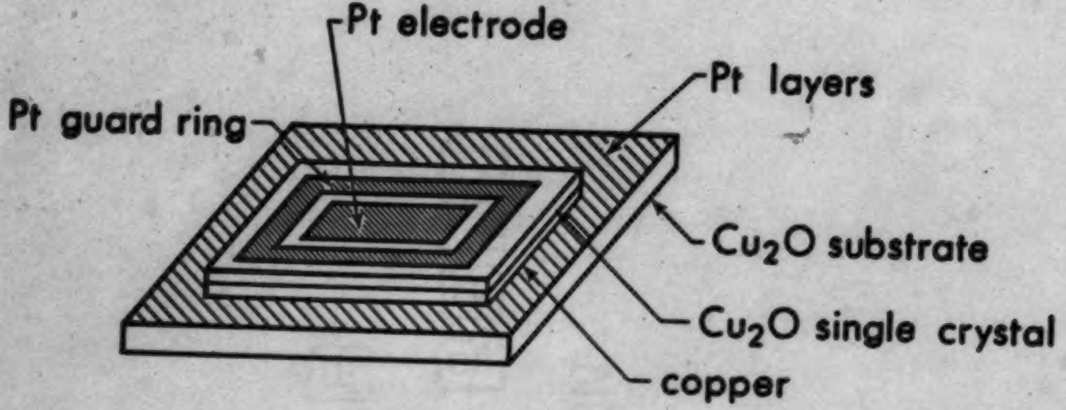
Pt electrode
Pt layers
Pt guard ring
Cu_2O substrate
Cu_2O single crystal
copper

Fig. 2a. A view of the structure of the Cu_2O single crystal diode, with platinium electrode and guard ring.

Fig. 2b. Cross section view of the Cu_2O single crystal diode, with platinium electrode and guard ring.

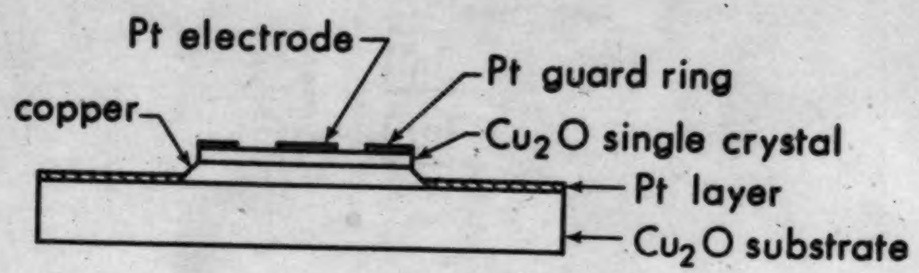
Pt electrode
Pt guard ring
copper
Cu_2O single crystal
Pt layer
Cu_2O substrate

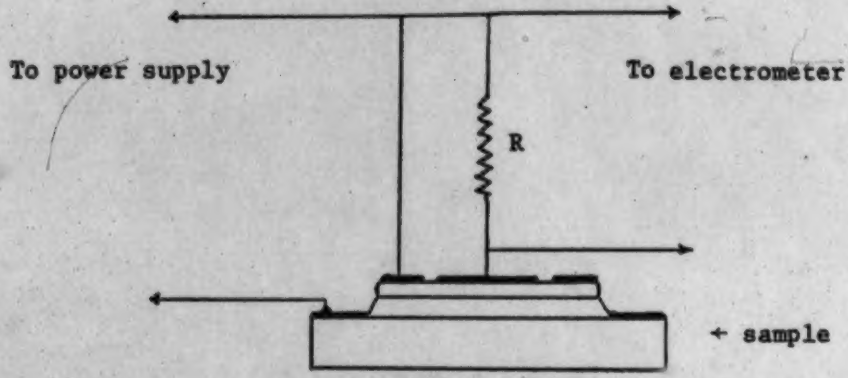
To power supply
To electrometer
R
← sample

Fig. 2c. A simplified diagram of the electrical circuit used for I-V measurement.

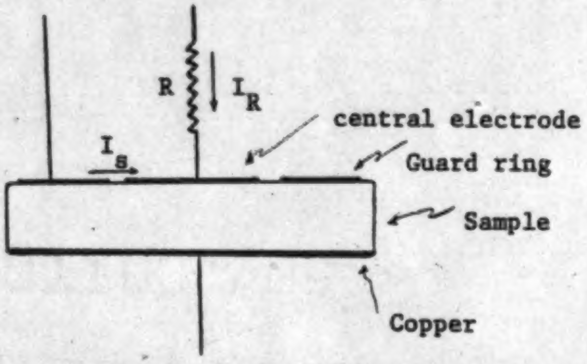
R
I_R
I_s
central electrode
Guard ring
Sample
Copper

Fig. 3. Diagram showing the current components for guard ring arrangement.

atmosphere. To achieve a vacuum of 10^{-6} torr, a pumping system consisting of a roughing pump and a mercury diffusion pump (Fig. 4) is used. A quartz capillary tube which can be heated to a higher temperature to allow extremely pure He gas to leak into the system is also attached to the system.

The sample chamber is shown in Fig. 5. The electrical leads to and from the sample are well-screened against outside interference. The sample is heated by a heating coil placed inside the copper tube which also serves as a sample holder.

After the sample has been preheated in vacuum, helium gas is allowed to leak into the system and the measurements of the current-voltage characteristics are carried out in helium atmosphere. The presence of helium gas in the system provides the necessary medium for heat transfer between the sample and external heating or cooling system and at the same time avoids the formation of the conducting layers on the sample surface.

The effectiveness of eliminating the surface current using this method is shown in Fig. 6 which gives the forward conductance with respect to temperature during the heating process. The data points ● are obtained without guard ring, while those points ○ are obtained with guard ring. The two upper curves are obtained while increasing temperature. As we can see the two curves merge at around

Fig. 4. A diagrammatic view of the vacuum pumping system.
(a) heater
(b) mercury diffusion pump
(c) quartz helium leak
(d) liquid nitrogen traps
(e) dewar flasks
(f) cold-cathode vacuum gauge

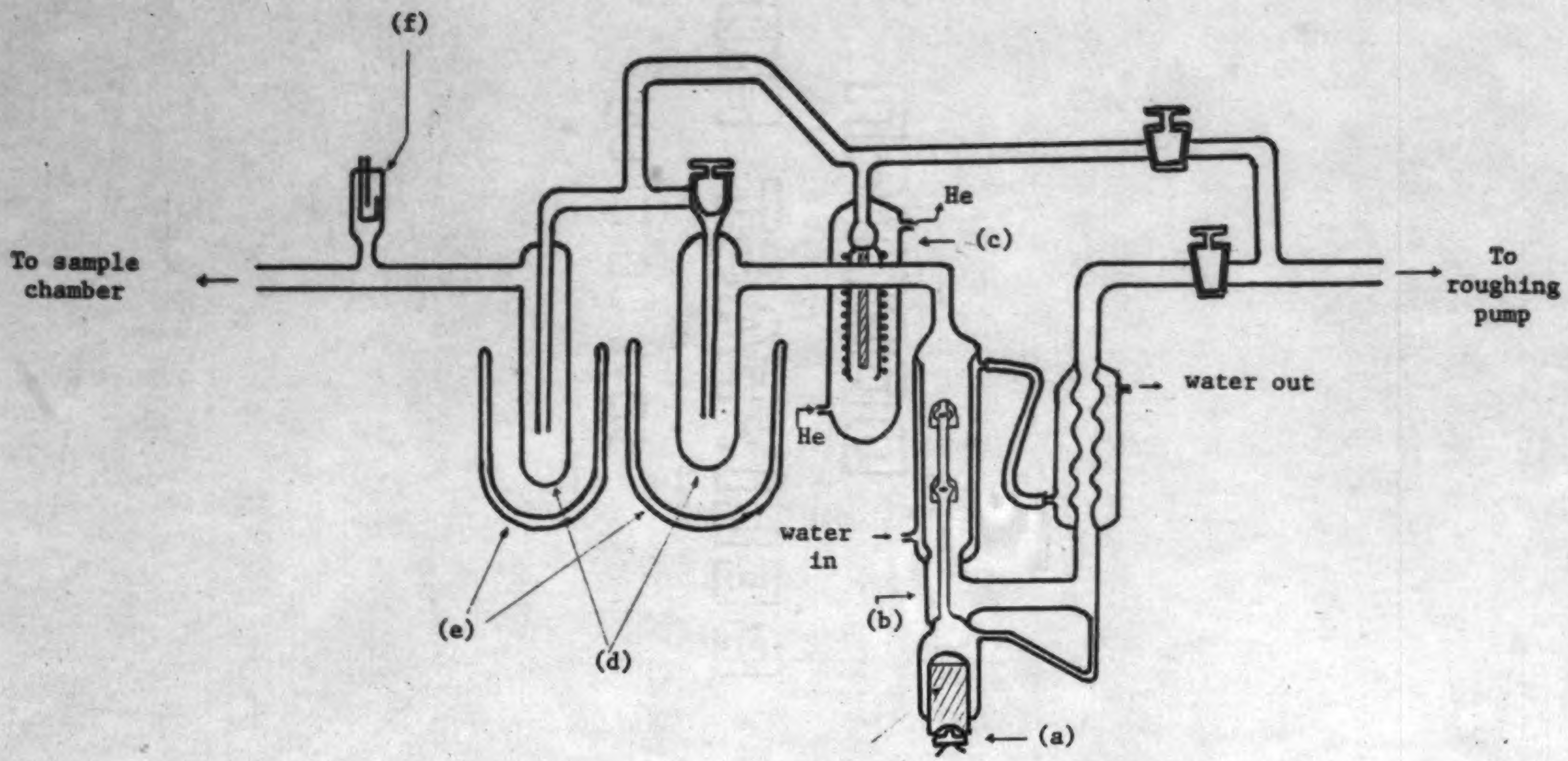
(f)
To sample chamber
He
(c)
To roughing pump
water out
He
water in
(b)
(e)
(d)
(a)

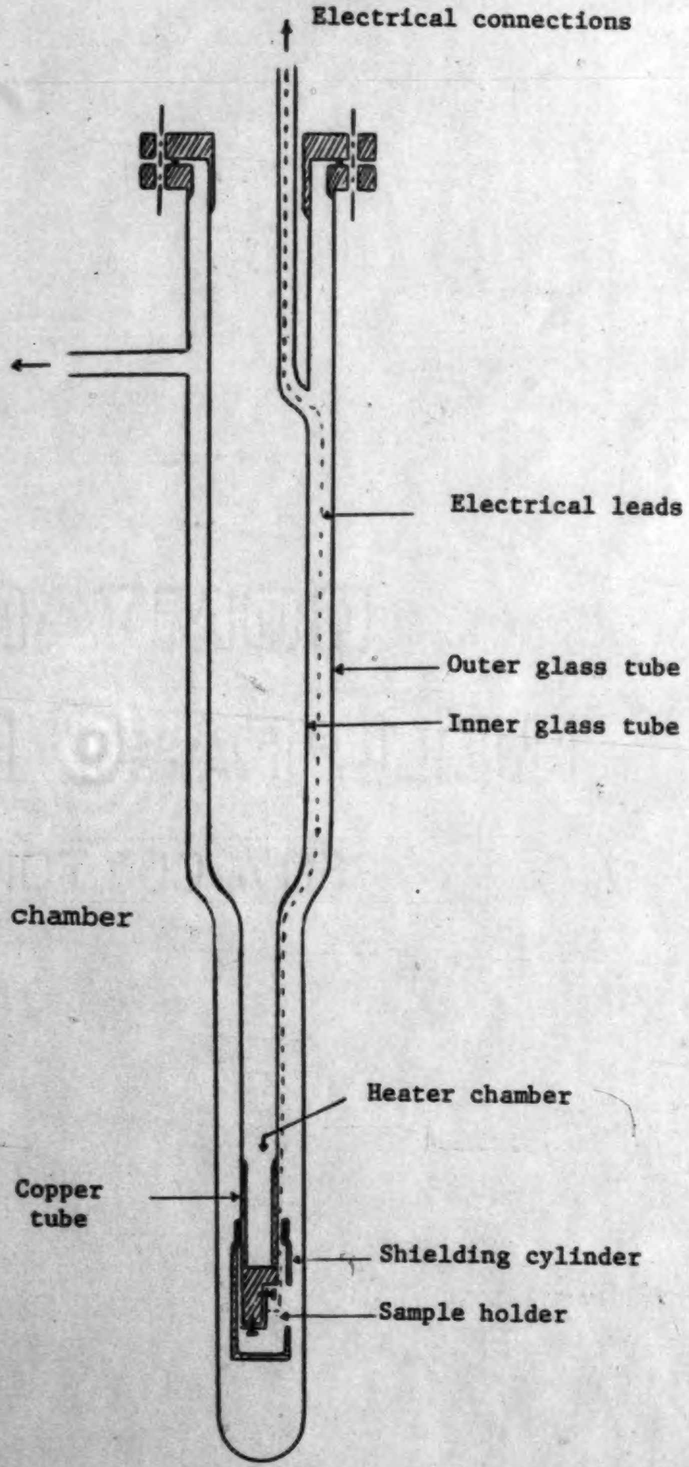
Electrical connections
To pumping system
Electrical leads
Outer glass tube
Inner glass tube
Heater chamber
Copper tube
Shielding cylinder
Sample holder

Fig. 5(a). Sample chamber

Fig. 5(b). Cross section of the sample holder.

Fig. 5(c). Top view of the sample holder.

Fig. 5(b)

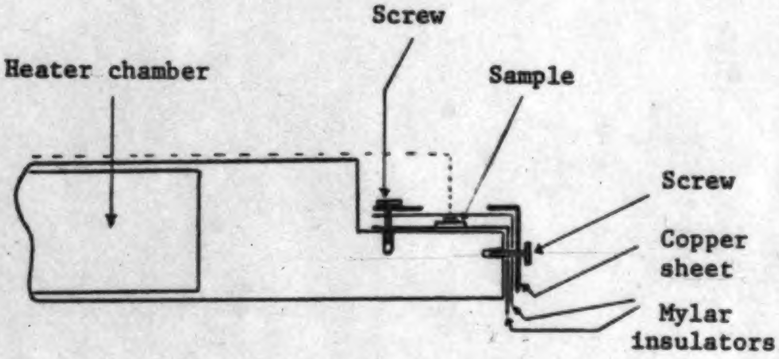
Screw
Heater chamber
Sample
Screw
Copper sheet
Mylar insulators

Fig. 5(c)

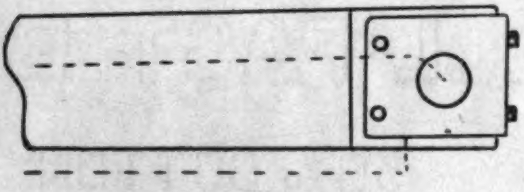

Note: Dashed lines represent electrical leads.

Fig. 6. The forward conductance of the Cu_2O single crystal diode (Sample SD-3) versus the reciprocal of the absolute temperature. The vertical axis is in logarithmic scale. The data points (●) were taken with temperature increasing (from room temperature to about 200°C) using guard ring technique, points (○) with temperature increasing (from room temperature to about 200°C) without the use of the guard ring, and points (Δ) with temperature decreasing (from 200°C to room temperature) with and without the use of the guard ring.

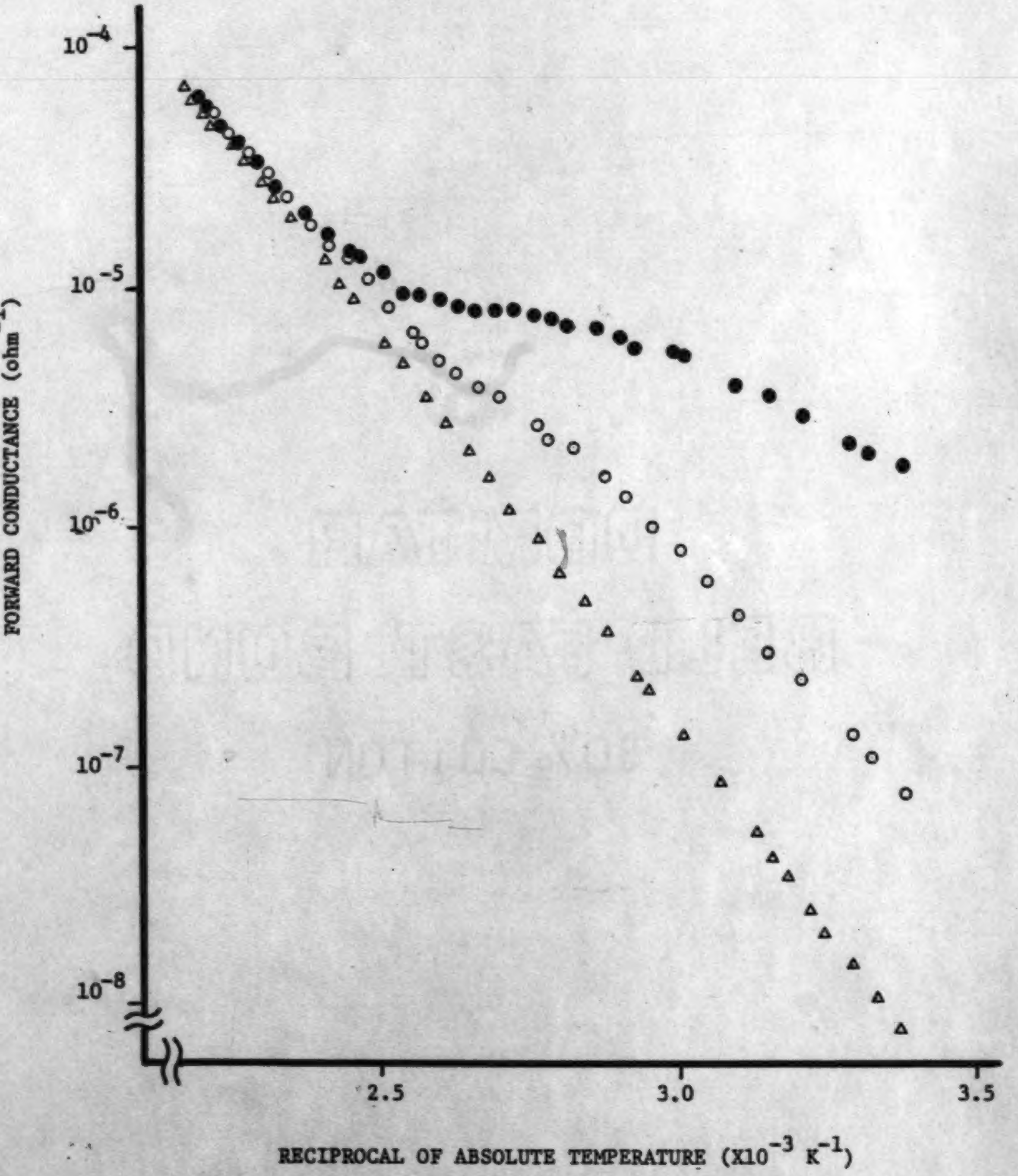
FORWARD CONDUCTANCE (ohm^{-1})
10^{-4}
10^{-5}
10^{-6}
10^{-7}
10^{-8}
2.5
3.0
3.5
RECIPROCAL OF ABSOLUTE TEMPERATURE (X10^{-3} K^{-1})

160°C, indicating the complete elimination of surface current. The change of slope in the middle curve (with guard ring) at about 100°C is well known to be due to the elimination of the photomemory effect (Kuzel 1961, Zouaghi et al. 1970, Tapiero et. al. 1976). Comparing the two upper curves indicates that the surface current of this particular sample before heating is more than one order of magnitude larger than the true bulk current.

After reaching about 200°C, the heating current is reduced slowly. When cooling, the currents measured with or without guard ring are identical, as shown in the lowest curve in Fig. 6 (data points Δ). This curve shows that the conductance in the cooling process exhibits the usual characteristics $\frac{1}{R} \alpha \exp(-\frac{E_a}{kT})$. The effectiveness of eliminating the surface current by vacuum pre-heating is therefore verified.

It should be noted here that the vacuum-preheating method eliminates both the surface current and photomemory effect, while the guard-ring method without preheating the sample only eliminates the surface current.

A Hewlett-packard DC power supply (model 6209 B) is used to provide voltages up to 300 volts. A Keithley 601 electrometer is used to measure the current. The temperature is measured by a chromel-alumel thermocouple attached to the Cu_2O crystal.

Chapter 3

The Pt-Cu_2O-Cu Structure as a Diode

(1) Introduction

Although our main research emphasis on the Pt-Cu_2O-Cu structure described earlier has been focused on the forward current-voltage characteristics which will be described in later chapters, the study of the possibility of using it as a rectifier of improved performance over the conventional Cu_2O-Cu rectifier was one of our early aims. Although we later found that the reversed current-voltage characteristics still exhibited certain undesirable effects, we feel that a brief description and discussion of the behaviour of this structure, especially in the reversed-biased condition is worthwhile here, since the sequence of material in this thesis follows more or less in accordance to the sequence of development of the project.

As part of our study of diode characteristics we also describe here measurements of the I-V characteristics of the diode before and after it has been heated up to 130°C for different periods of time. These serve as a test for the suggestion made by Weichman and Kuzel (1970a) on the deterioration of reversed current which we described in chapter 2.

(2) The effect of oxidation on the I-V characteristics of the diodes:

The starting Cu_2O single crystal has a resistivity of 10^7 ohm-cm or higher. After the Cu_2O crystals and copper are bonded together and the Cu_2O single crystal is polished down to about 200 μm, the current-voltage characteristics of the sample are measured both before and after oxidation.

Fig. 7 shows the I-V characteristics of one of the diodes (sample S-9), whose central electrode area was 5.7 x 5.7 mm^2, before oxidation. The reversed current is close to ohmic in its behaviour. The Cu-Cu_2O junction, although blocking at higher voltage (not shown in Fig. 7), can provide the carriers required at low voltage, i.e. it is ohmic in nature at low voltage as shown in Fig. 7. Since the bulk resistance is very high, the ratio of reversed-forward resistance is close to unity.

At higher voltages, the reversed current shows a very serious creeping effect which is shown in Fig. 9 and will be described in a later section.

Fig. 8 shows the I-V characteristics of the same sample after oxidation. Although both the forward and reversed currents increase after oxidation (oxidized at 1-2 torr of air at about 600°C for about 10 hours), the forward current has a more dramatic increase (of the order of 100 times). For this particular sample, a forward-reversed

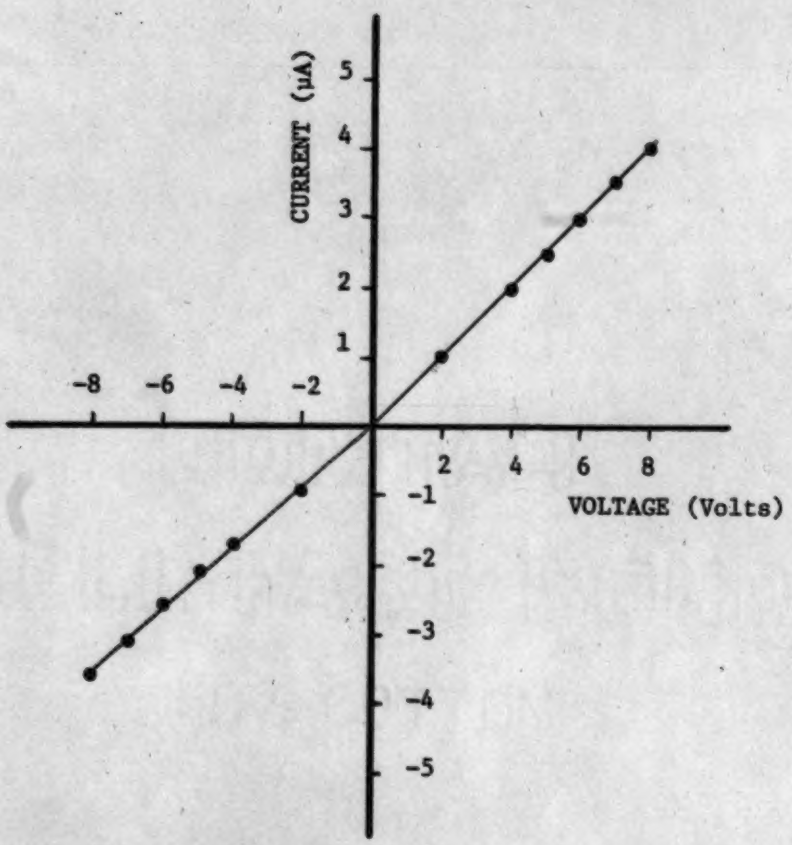

Fig. 7. The current-voltage characteristic of sample S-9 before oxidation, measured by guard-ring method. T=298°K.

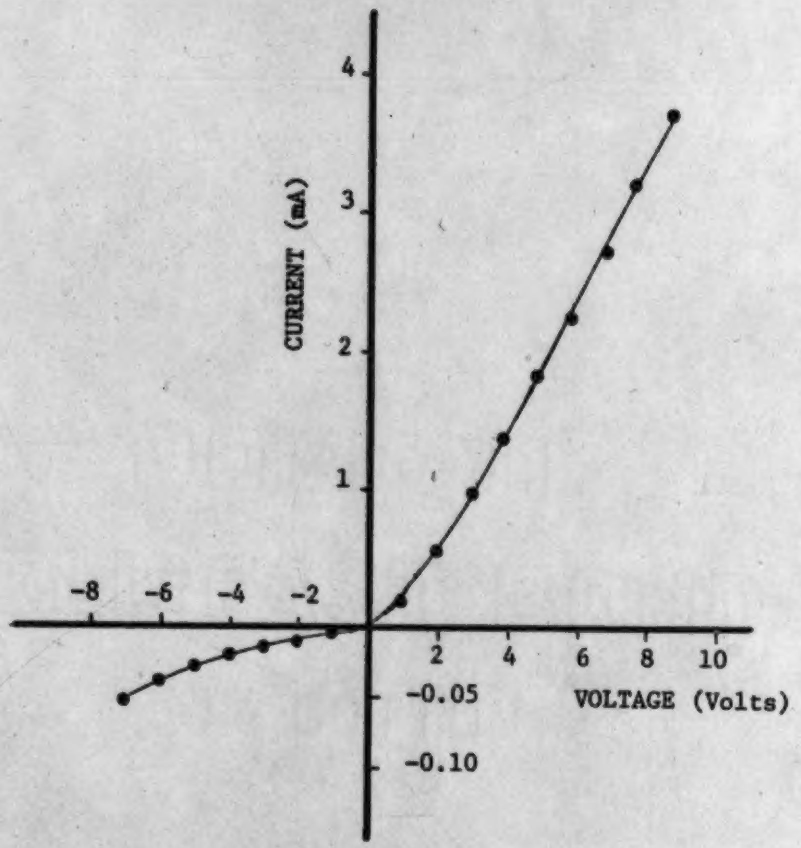

Fig. 8. The current-voltage characteristic of sample S-9 after oxidation, measured by guard-ring method. (The scale on the upper half of the ordinate is different from that of the lower half.) T=298°K.

current ratio of about 60 is obtained at an applied voltage of 5 volts.

Cu_2O has long been known to be a deficit, p-type semiconductor (Mott and Gurney 1940, Bloem 1958). The decrease in resistance after oxidation is due to the increase of defects (or more specifically, Cu^+ vacancies). The Cu^+ vacancies result in localized acceptor states. Electrons from the valence band are excited into these localized states leaving mobile holes behind, which in turn results in much higher forward current. The reverse current remains limited by the junction.

(3) Reversed current-voltage characteristics:

For practical uses, it is required that a diode has a high resistance under reversed bias condition. Any large deterioration of reversed current with respect to time is therefore undesirable. Conventional Cu_2O rectifiers are well known to exhibit some undesirable effects in the reversed direction which we have already described in chapter 2.

The reversed current of the rectifiers, made by the method described in the previous chapter, unfortunately still shows the creeping effect at higher applied voltages. As a constant voltage is applied in the reversed direction, the current starts to climb as time progresses. Fig. 9 shows an example of this type of creeping at various voltages.

At low voltages, the reversed current returns to the same initial current after the voltage has been switched off. This is shown in Fig. 10, where curve 1 was measured with constant voltage of 30 volts applied on the sample. After about 1½ hours, the voltage was switched off (refer to Fig. 10). Curve 2 in Fig. 10 was traced with the voltage on only for a few seconds, just long enough to measure the current but short enough to avoid further serious creeping. Curve 2 shows the decay of reversed current to its original value.

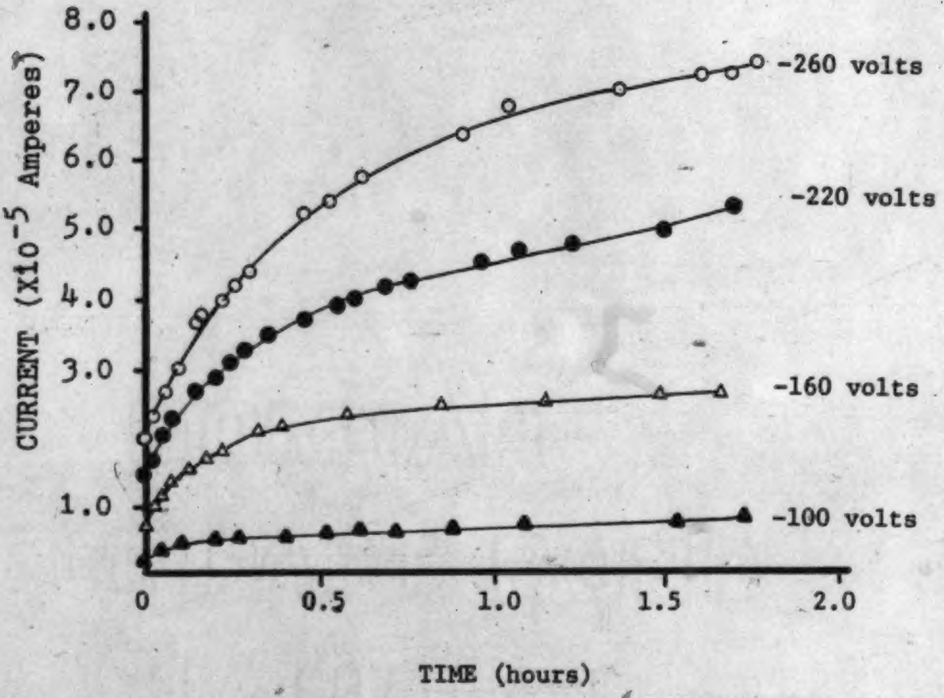

Fig. 9. The reversed current versus the duration of reversed voltage. (Sample SD-5)

Fig. 10. The reversed current at 30 volts versus elapsed time. Curve (1) is taken with reversed voltage applied continuously and curve (2) is taken with reversed voltage applied for only a period of a few seconds to take current reading. (Sample SD-5)

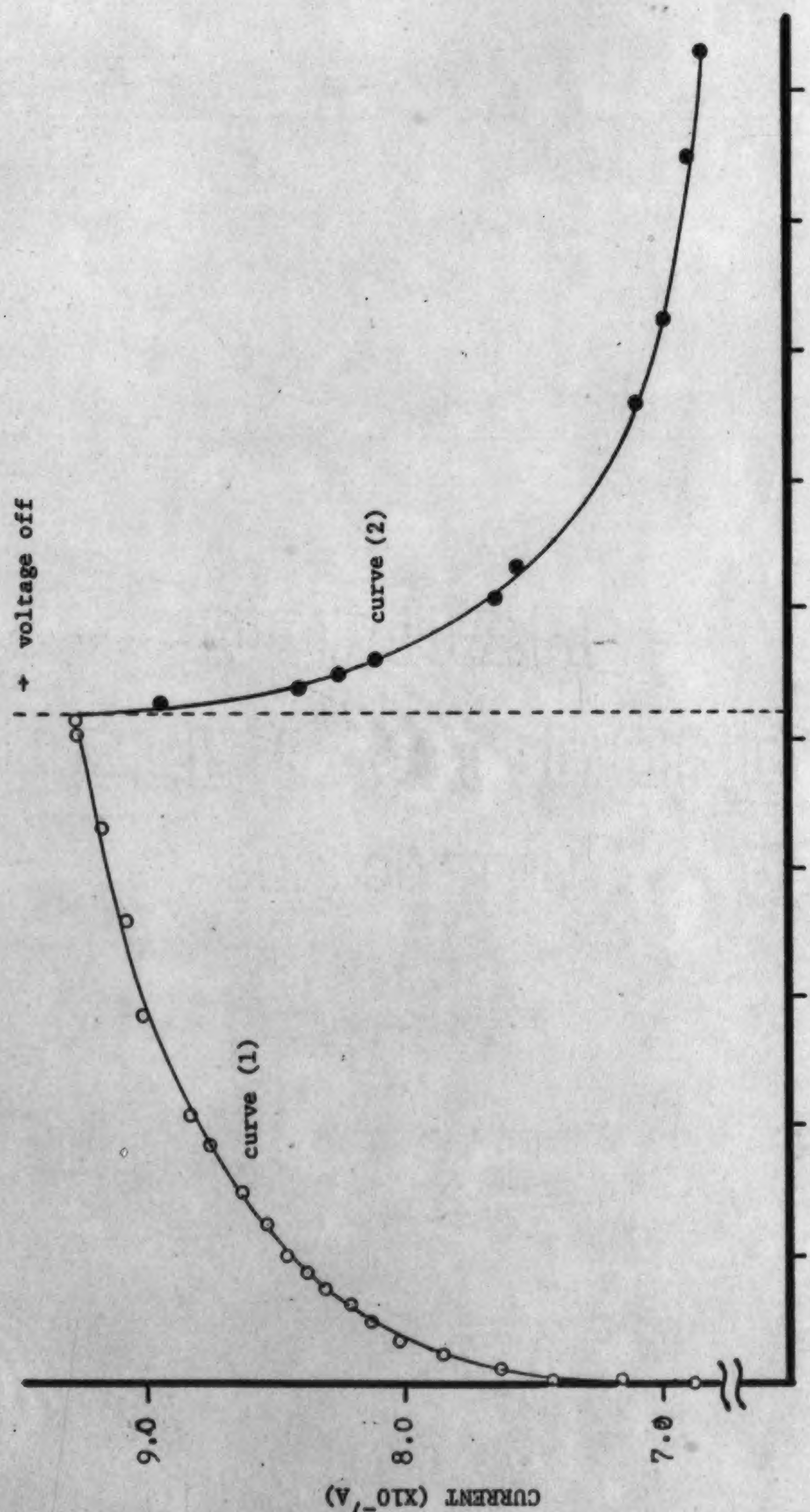
← voltage off
curve (1)
curve (2)
CURRENT (X10^{-7}A)
9.0
8.0
7.0
TIME (X10^{3} seconds)
1
2
3
4
5
6
7
8
9
10

The creeping effect still exists after oxidation. For conventional Cu_2O rectifiers, Kuzel (1961) reported that a brief heating (≈ 10 minutes) at 130°C could stabilize the reversed current, but excessive heating (an hour or more) caused a serious deterioration of the reversed current. The explanation, that the multicrystalline grain boundaries were responsible for this later deterioration, was mentioned in chapter 2.

To examine the validity of the explanation, tests were carried out by exposing our single-crystal diodes to the same heat treatment. Fig. 11 shows two I-V curves after different heating periods at 130°C in air. Heating did stabilize the reversed current somewhat, but a complete stability was not achieved.

It was also found that excessive heating (up to 2 hours or more) on the Cu_2O single crystal diode had no undesirable effect on the reversed current (Fig. 11) as had been reported for the conventional diodes. This supports the suggestion of Kuzel that grain boundaries are responsible for the deterioration after excessive heating in the case of conventional multicrystalline Cu_2O rectifiers.

Fig. 11. The effect of heating at 130°C in air on the current-voltage characteristics of Cu_2O single-crystal diodes. Points (•) are taken before heating at 130°C in air, and points (×) are taken after heating for 2 hours at 130°C in air. (The scale on the upper half of the ordinate is different from that of the lower half.)

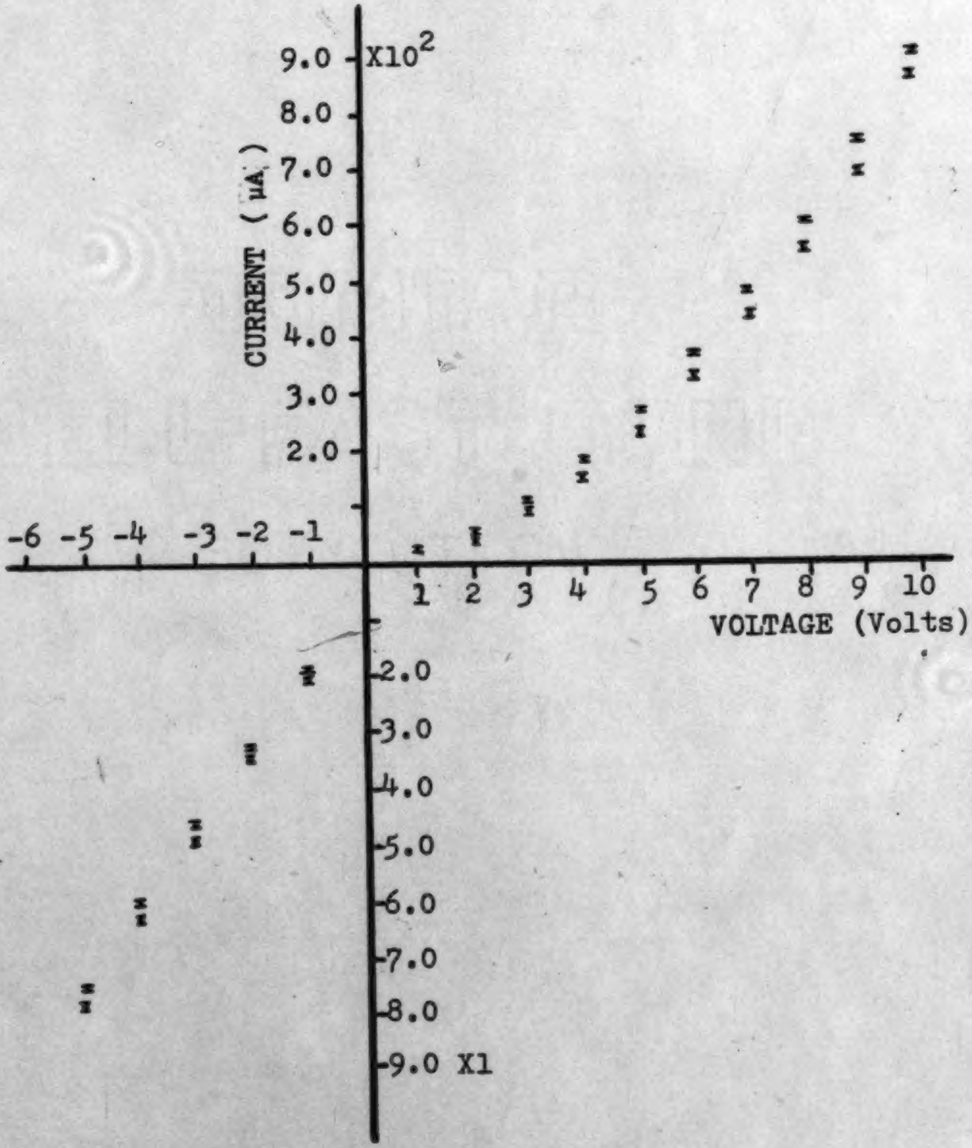

(4) Conclusion:

Measurements on the reversed current of the Cu_2O single crystal diodes have supported the suggestion that some of the deterioration of conventional multicrystalline Cu_2O rectifiers are due to the existence of grain boundaries.

The sample shown in Fig. 8 has a resistivity of 10^4 ohm-cm. Although lower resistivity has been reported for Cu_2O, especially in the early literature (Grondahl 1933), it is not clear that the reported resistivities represent that of the bulk material. Surface and grain boundaries tend to have lower resistivity (Weichman and Kuzel 1970a, Kuzel and Weichman 1970). In my own experience, 10^4 ohm-cm is the lowest bulk resistivity that I have observed for Cu_2O single crystal. Results obtained by the Cu_2O research group in Strasburg (Zielinger et. al. 1972) appear to indicate the same. Thus the forward resistance (few kilo-ohms) for the sample shown in Fig. 8 appears to be close to the lowest value we can get for the given thickness ($\approx$ 200 μm) and area ($\approx 5.7 \times 5.7$ mm^2). This higher forward resistance is undesirable for practical applications.

Furthermore, the creeping effect, though it can be reduced by heating at 130°C, cannot be completely eliminated.

Chapter 4

Pt-Cu_2O-Cu Single Injection Diodes

(1) Introduction

In Chapter 2 we described our method of making Cu_2O-Cu diode structures. This and the following chapter will give the results on the study of the forward I-V characteristics of these diodes.

As mentioned earlier, after the Cu_2O crystal has been bonded to the copper, the diode structure is subject to further heat treatment. One set of diodes was annealed in high vacuum ($\approx 10^{-6}$ torr at 800°C) and the other set annealed at higher air pressure ($\approx$ 1-2 torr at 600°C). We shall, from now on, refer to the first set as the vacuum-annealed samples, and the second as the oxidized samples.

It was found that the diodes annealed in different conditions have very different characteristics. It was first thought that annealing of these diodes in different conditions would only result in a change in the localized states in the bulk of the crystal, as had been found in previous studies on Cu_2O crystals (Bloem 1958, Weichman and Kuzel 1970b, Zielinger et. al. 1972). However, experimental results indicate that, aside from this change in localized states in the bulk, the Cu-Cu_2O junction has also been affected. Certain phenomena, such as negative resistance, appear only in oxidized samples. This, together with other experimental results, indicates that double injection, i.e. the injection of holes from the Pt electrodes and electrons from the Cu-Cu_2O junction, is responsible for the I-V characteristics observed in oxidized samples. The vacuum-annealed samples, however, show the characteristics of one-carrier injection, i.e. injection of holes from Pt electrodes only. This forces us to the conclusion that annealing at the higher air pressure converts the Cu-Cu_2O junction to a more efficient electron-injecting electrode.

We shall give, in this chapter, the theory on one-carrier space-charge-limited conduction and the experimental results on the vacuum-annealed samples. Conclusions can be drawn from these results regarding the distribution of localized states in the bulk of Cu_2O crystal.

The oxidized samples, on the other hand, will be discussed in the next chapter, together with the theory on double injection.

We should mention here that all the I-V characteristics discussed in the following two chapters (chapters 4 and 5) are for the forward biased condition unless specified otherwise.

(2) Theory on one-carrier space-charge-limited conduction:

In deriving Ohm's law in solids, the condition of charge neutrality is always assumed. In this case, the thermally excited carriers are the free carriers whose motion constitute the current. The potential distribution between the electrodes is approximately linear. As a result, the current density is given by

$$J = e\,(n_o\mu_n + p_o\mu_p)\,\frac{V}{L} \tag{4-1}$$

or, $J \alpha V$

If only one type of carrier (either electrons or holes) is injected into a semiconductor or insulator, it is obvious that space charge will build up inside the bulk as each injected carrier contributes one excess electronic charge to the solid. This can occur if one of the electrodes is an electron-injecting contact and the other a hole-blocking contact or vice versa. When the density of injected carriers becomes comparable or larger than the density of thermally excited carriers inside the solid, the charge neutrality condition, which is a requirement for the observation of ohmic conduction, will not hold. Deviations from ohm's law will then be observed.

A simple analogy of the build up of space charge inside solids as discussed above occurs in vacuum tube diodes. Electrons are injected from the heated cathode and, under an applied voltage, are accelerated towards the anode. When the density of injected electrons is high, space charge builds up in the vacuum space between cathode and anode. For the sake of convenience in comparison with the case of semiconductors later, the starting equations for space-charge-limited (SCL) conduction in vacuum are:

Poisson's equation,

$$\frac{d^2V}{dx^2} = \frac{en}{\varepsilon_o} \tag{4-2}$$

Conservation of energy for each electron,

$$\tfrac{1}{2}mv^2 = eV \tag{4-3}$$

Current equation,

$$J=env \tag{4-4}$$

The solution for the current-voltage characteristics in this case are well known to be the Langmuir-Child's law or three-halves power law:

$$I\alpha V^{3/2} \tag{4-5}$$

The principle of space charge conduction in semiconductors is similar to that of vacuum tube diodes, though there are differences in detail. Fig. 12 shows the band diagram of semiconductor and that of the metal contacts. The semiconductor is assumed to be p-type.

In the figure, holes are injected from the anode into the valence band of the semiconductor. These injected carriers, together with the thermally excited ones, are responsible for the current flow under applied voltage.

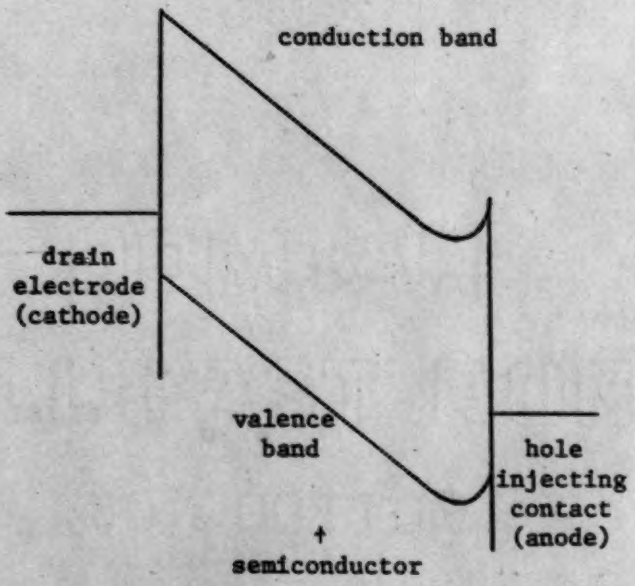
conduction band
drain
electrode
(cathode)
valence
band
hole
injecting
contact
(anode)
semiconductor

Fig. 12. Schematic energy-band diagram of a p-type semiconductor under forward bias condition. Holes are injecting from the anode.

Although the overall picture is similar to that of vacuum tube diodes, there are several additional factors that should be taken into consideration in the case of semiconductors.

(a) At a given temperature, there are a substantial number of thermally excited free charge carriers inside the crystal.

(b) There are collisions of charge carriers with thermal vibrations of the host lattice (phonons), and with chemical impurities and structural imperfections in the crystal.

(c) There are, inside the band gap, localized energy states that act as traps for the charge carriers.

The existence of thermally excited carriers results in the occurrence of ohmic conduction at low applied voltages, when the density of injected carriers is small. For perfect crystal, deviation from Ohm's law occurs when,

$$\bar{p}_i = p_o \tag{4-6}$$

where $\bar{p}_i$ is the average density of injected holes, and p_o the density of thermally excited carriers.

The total injected charge can be roughly estimated as,

$$Q_i = CV = \varepsilon \frac{A}{L} V$$

where C is the capacitance of the sample, V the applied voltage, ε the dielectric constant, A the area of the injecting electrode, L the thickness of the sample.

The average density of injected charge carriers will then be,

$$\bar{p}_i = \frac{Q_i}{eAL} = \frac{\varepsilon V}{eL^2}$$

Thus condition (4-6) gives,

$$\frac{\varepsilon V_t}{eL^2} \approx p_o$$

where V_t is the transition voltage between the ohmic conduction regime and the space-charge-limited conduction regime.

Thus, $$V_t \approx \frac{eL^2 p_o}{\varepsilon} = \frac{L^2}{\rho \varepsilon \mu} \quad \text{(for a perfect crystal)}$$

where ρ is the resistivity of the crystal and μ the mobility of the carriers.

Because of collisions of carriers with phonons, impurities and defects, the relation $\frac{1}{2}mv^2 = eV$ cannot be used here. Instead, the relation between velocity and field $\vec{v} = \mu \vec{E}$ should be used. The mobility μ is approximately constant at low field and depends on $\vec{E}$ at high fields in most cases.

It is well known that, in solids, some impurities and defects can result in the existence of localized energy states within the band gap. These states can act as traps for charge carriers. As a result, not all injected carriers contribute to the current since the charge carriers can occupy these localized (trapping) states for non-negligible length of time.

The current-voltage characteristics for space-charge-limited (SCL) conduction in semiconductors can be obtained in the same way as that of vacuum tube diodes. As mentioned earlier, because of collisions, the relation $\frac{1}{2}mv^2 = eV$, used in the case of vacuum tube diodes, cannot be used. Instead, the relation $\vec{v} = \mu \vec{E}$ should be used.

The current equation is given as,

$$J = epv - eD \frac{dp}{dx} \tag{4-7}$$

The diffusion term, $- eD \frac{dp}{dx}$, is very often neglected, as it is important only near the injecting electrode. As a result, the current equation is approximately given by,

$$J \simeq epv \tag{4-8}$$

The current-voltage characteristic of SCL conduction in solids depends on the trap distribution. A few cases are considered as follows:

(a) Perfect trap-free semiconductors:

This is the simplest idealized case in solids. The starting equations are:

$$\frac{\varepsilon}{e} \frac{dE}{dx} = p \tag{4-9}$$

$$v = \mu E \tag{4-10}$$

$$J = epv \tag{4-11}$$

and the boundary condition is taken as

$$E = 0 \text{ at } x = 0 \tag{4-12}$$

where the injecting contact is taken at $x = 0$.

The solution for current-voltage characteristics is,

$$J = \frac{9}{8} \varepsilon\mu \frac{V^2}{L^3} \tag{4-13}$$

or,

$$J \alpha V^2 \tag{4-14}$$

For the case of field-dependent mobility of the form,

$$\mu(E) \ \alpha \ E^{-\frac{1}{2}} \tag{4-15}$$

The current-voltage characteristic is given by (Lampert and Mark, 1970) :

$$J\alpha V^{3/2} \tag{4-16}$$

(b) Semiconductors with traps:

In real solids, it is understandable that the existence of traps can affect the current-voltage characteristics as some of the injected carriers are trapped and do not contribute to the current.

In this case, the right hand side of Poisson's equation should include an additional term, the density of trapped carriers p_t. Thus the starting equations are,

$$\frac{\varepsilon}{e}\frac{dE}{dx} = p + p_t \tag{4-17}$$

$$v = \mu E \tag{4-18}$$

$$J = epv \tag{4-19}$$

To solve the above equations, we need additional information about the relation between p and p_t. This is where the trap distribution comes into the problem. The case of single-level shallow traps (Fig. 13) and also the

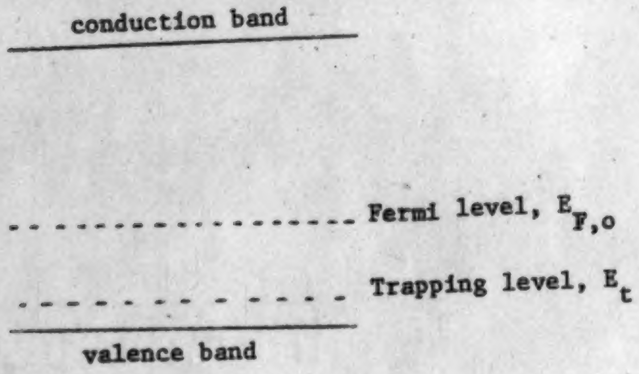
conduction band
Fermi level, $E_{F,o}$
Trapping level, E_t
valence band

Fig. 13. Schematic energy-band diagram of a semiconductor with shallow traps at energy E_t.

$(\frac{E_F-E_t}{kT} >> 1)$

case of a distribution of traps following an exponential decrease in density with energy, as sketched in Fig. 14, are considered below.

(i) Semiconductors with single-level shallow traps:

Consider the case of semiconductor with a hole trap, E_t, which lies below the quasi-Fermi level E_F, in such a way that,

$$\frac{E_F-E_t}{kT} >> 1 \qquad (4\text{-}20)$$

A hole trap satisfying this relation is said to be shallow.

Also the density of free carriers is given by,

$$p = N_v \exp\left(-\frac{E_F-E_v}{kT}\right)$$

The density of trapped carriers is given by,

$$p_t = \frac{N_t}{1 + \frac{1}{g}\exp\left[-\frac{(E_t-E_F)}{kT}\right]}$$

where N_t is the density of traps, and g the degeneracy factor.

For $(E_F-E_t)/kT >> 1$, we have

$$\frac{p}{p_t} = \frac{N_v}{gN_t}\exp\left(-\frac{E_t-E_v}{kT}\right) = \theta \qquad (4\text{-}21)$$

This is the additional constraint required to solve the problem.

Using (4-17) and (4-21), we have,

$$\frac{\varepsilon}{e}\frac{dE}{dx} = \left(1 + \frac{1}{\theta}\right) p \qquad (4\text{-}22)$$

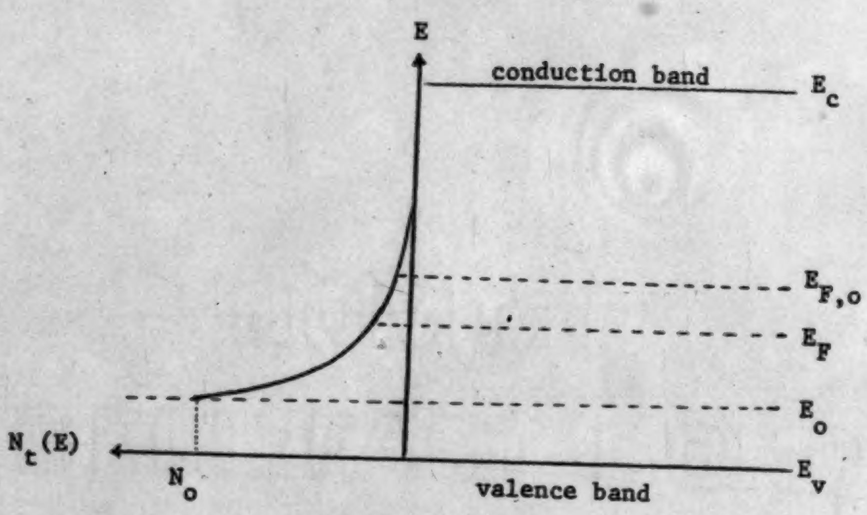
E
conduction band
E_c
$E_{F,o}$
E_F
E_o
$N_t(E)$
N_o
valence band
E_v

Fig. 14. Schematic energy-band diagram of a semiconductor with a distribution of traps following an exponential decrease in density with energy.
($E_{F,o}$: Fermi level at thermal equilibrium.
E_F : quasi-Fermi level.)

In practice, most of the charge carriers are trapped. The factor $1/\theta$ is usually very large. As a consequence, we have, from (4-22),

$$\frac{\varepsilon}{e}\frac{dE}{dx} \approx \frac{1}{\theta}\,p \qquad (\text{for } \frac{1}{\theta} >> 1) \qquad (4\text{-}23)$$

By solving (4-18), (4-19) and (4-23), we have the current-voltage characteristic, for the case of shallow trapping, given by,

$$J = \frac{9}{8}\,\theta\varepsilon\mu\,\frac{V^2}{L^3} \qquad (4\text{-}24)$$

The functional relation between J and V is the same as that of perfect solids, i.e. $J\alpha V^2$. However, since the factor θ is usually very small, the SCL current in this case is much smaller than that of perfect solids.

(ii) Semiconductors with traps of exponential distribution:

Again, we need an additional relation between p and p_t in order to solve the equations (4-17), (4-18) and (4-19).

Consider a trap density distributed in the form,

$$N_t(E) = N_o \exp\left[-\frac{E-E_o}{kT_c}\right]$$

where T_c is the characteristic temperature which determines the rate at which density of states decreases as energy increases, E_o the lowest energy traps, and N_o the density of traps at that energy. Fig. 14 shows the variation of states with respect to energy.

The density of filled hole traps,

$$p_t \approx \int_{E_o}^{\infty} \frac{N_o \exp\left(-\frac{E-E_o}{kT_c}\right)}{1 + \exp\left(\frac{E_F-E}{kT}\right)}$$

$$\approx \int_{E_F}^{\infty} N_o \exp\left(-\frac{E-E_o}{kT_c}\right)$$

$$= N_o\, kT_c \exp\left(-\frac{E_F-E_o}{kT_c}\right)$$

The density of free holes,

$$p = N_v \exp\left(-\frac{E_F-E_v}{kT}\right)$$

Thus, we have

$$p \alpha p_t^{\frac{T_c}{T}} \qquad (4\text{-}25)$$

Using (4-25), together with (4-17), (4-18) and (4-19), the solution for I-V characteristics in this case can be shown to be

$$J = N_v \mu_p e^{(1-\ell)} \left[\frac{\varepsilon \ell}{N_s(\ell+1)}\right]^{\ell} \left(\frac{2\ell+1}{\ell+1}\right)^{(\ell+1)} \frac{V^{\ell+1}}{L^{2\ell+1}} \qquad (4\text{-}26)$$

where $\ell = \frac{T_c}{T}$, and $N_s = N_o kT_c \exp\left(\frac{E_o-E_v}{kT_c}\right)$.

The detailed procedure for solving the equation was given by Mark and Helfrich (1962).

The relation $J \alpha V^{\ell+1}$ was first obtained by Rose (1955). A more exact form was derived by Mark and Helfrich (1962).

Comparing (4-24) and (4-26), we see that a single discrete level gives a $J \alpha V^2$ relation, while an exponential distributed trap gives a higher power relation, $J \alpha V^{\ell+1}$ ($\ell = \frac{T_c}{T} > 1$). Thus, if the conduction mechanism has been established from other experimental results to be a single-carrier space-charge-limited conduction, we can deduce the type of localized states inside the crystal from the I-V relation. This method has been proved to be very powerful in the past as a probe for the localized states inside semiconductors or insulators.

In the following, we shall show that single-carrier space-charge-limited conduction is the mechanism involved in the vacuum-annealed Cu_2O diodes. The type of localized states in the bulk are then discussed.

(3) Experimental results - vacuum-annealed samples

3-1 Introduction

The electrical properties of Cu_2O have long been known to depend on the way it has been heat-treated. Annealing at high vacuum or in a gas mixture with low oxygen partial pressure was found to create high resistivity, while annealing in gas mixture with higher oxygen partial pressure was found to have lower resistivity. This is usually explained by the variation of the density of Cu^+ vacancies inside the crystal when annealed in different oxygen partial pressure. It was accepted that each Cu^+ vacancy results in an acceptor state and the density of Cu^+ vacancies depends on the previous heat treatment the crystal has received. Although this concept of single-level acceptor states due to Cu^+ vacancies was able to explain some experimental results in the past, it failed to account for others, such as why there is a wide variation of activation energies (from about 0.1 ev to about 1 ev) from one crystal to another (Zielinger et. al. 1972). The experimental results by Zielinger et. al. also showed the activation energies, E_a, and the resistivity at room temperature, ρ, of the crystals are more or less related as follows,

$$\rho \propto \exp(\beta E_a) \qquad (4\text{-}27)$$

which is sometimes called the Meyer-Neldel rule. The results of Zielinger et. al. are shown in Fig. 15. Noguet et. al. (1974) attempted to account for the wide variation

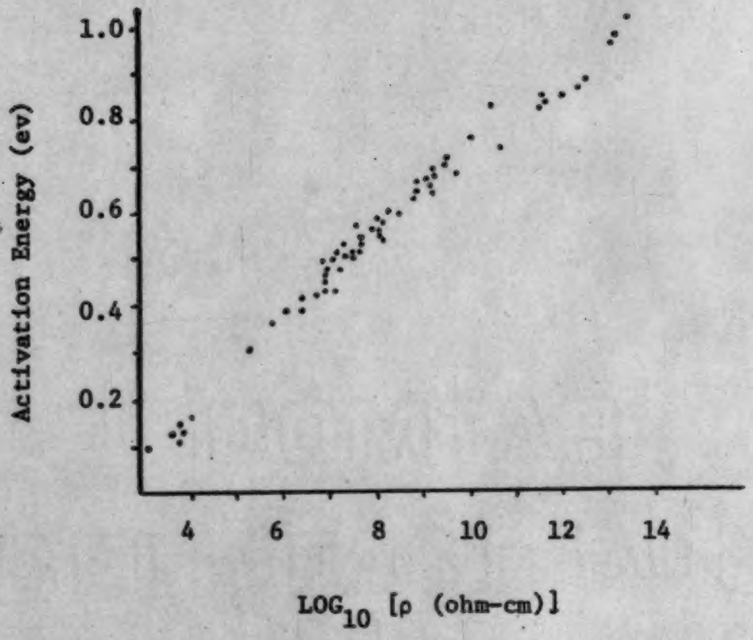

Fig. 15. The activation energies of Cu_2O crystals versus their corresponding resistivity at 20°C. (After Zielinger et. al. 1972).

of activation energy by assuming a continuous distribution of acceptor states. They also pointed out that the results on the optical absorption coefficient obtained by Prevot on Cu_2O support their assumption.

The discussion in section 2 of this chapter has clearly shown that the type of localized trapping states for majority carriers in a crystal can be probed by injecting majority carriers into the crystal and observing I-V characteristics in the space-charge-limited (SCL) conduction regime. Since, under injection condition, acceptor states can serve as hole traps for the injected holes, a probing of the acceptor states in Cu_2O by the method of single carrier injection can be achieved in suitable structures.

As we will report below, experimental results on the vacuum-annealed Cu_2O diodes show explicitly the characteristics of SCL conduction due to one carrier injection. The study of the I-V characteristics of these samples can therefore reveal the type of localized states in the bulks of these samples.

The following sections are intended to establish the fact that SCL conduction due to one-carrier injection is responsible for the I-V characteristics of the vacuum-annealed samples. This is achieved through the following observations:

(i) A transition from ohmic conduction to a regime with current and voltage in higher power relation is observed.

(ii) The relation between the current and the thickness of the Cu_2O single crystal at fixed voltage, in the regime where I and V are related by higher power relation, closely agree with theoretical prediction for the injection regime.

(iii) The study of the effect of photomemory on the I-V characteristics of the diode also suggested that the I-V characteristics are those of injection diodes.

(iv) A pulse test established that the conduction is due to one-carrier injection rather than two carrier injection.

We shall now discuss the above experimental results in detail.

3.2 Forward I-V characteristics of vacuum-annealed samples:

The I-V characteristics reported below were obtained after the sample had been preheated in vacuum at about 200°C to eliminate the surface current (i.e. by the vacuum-preheating method described in chapter 2). Measurements were carried out with samples kept in He atmosphere.

Fig. 16 shows the I-V characteristics of sample SD-10 at a temperature of 270°K. An ohmic region is clearly seen at lower voltages. At about 30 volts, a deviation

Fig. 16. The forward I-V characteristic of vacuum-annealed sample SD-10 at a temperature of 270°K.

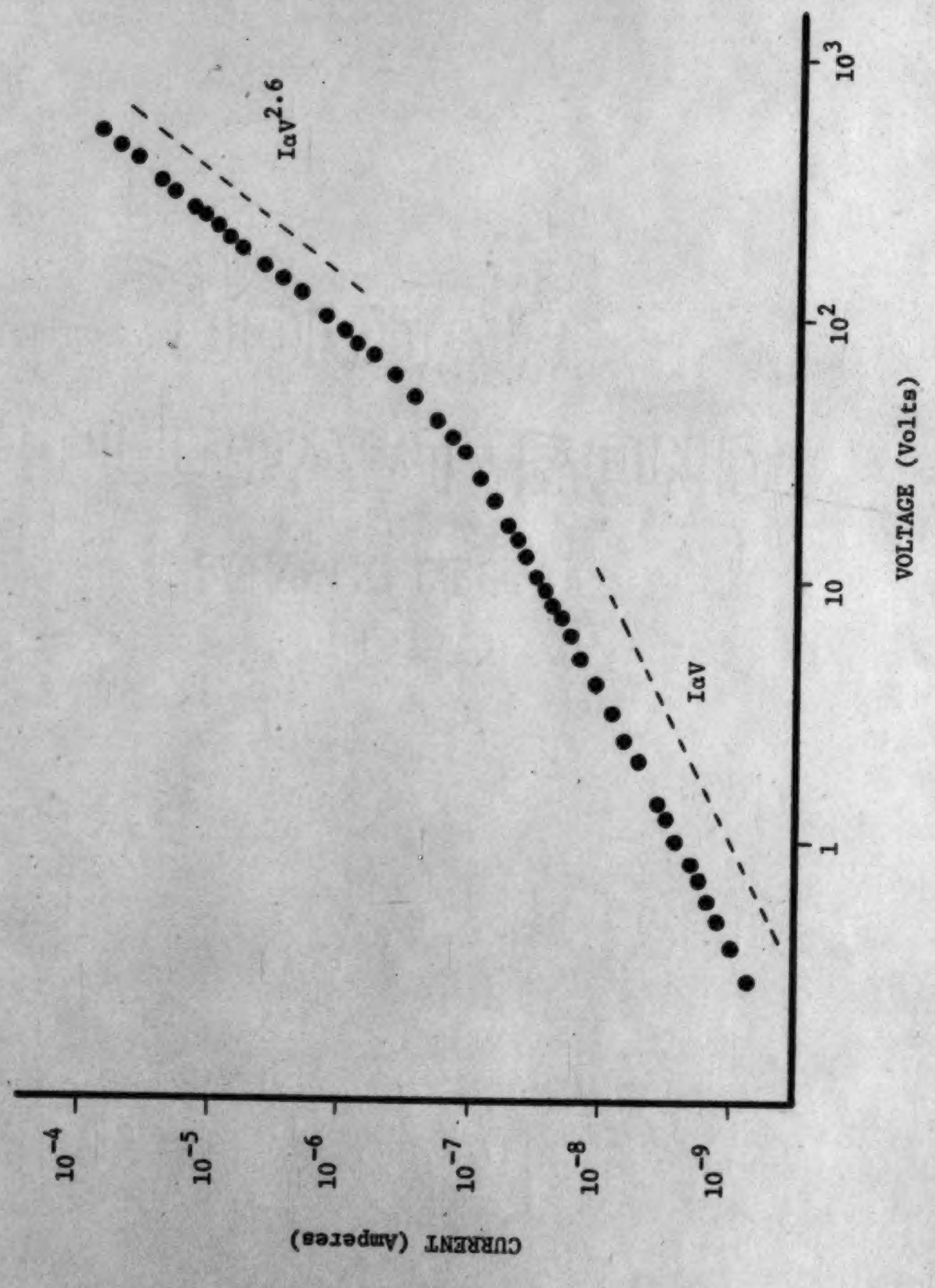
CURRENT (Amperes)
10^{-4}
10^{-5}
10^{-6}
10^{-7}
10^{-8}
10^{-9}
VOLTAGE (Volts)
1
10
10^2
10^3
$I \alpha V^{2.6}$
$I \alpha V$

from Ohm's law is observed. After a short transition, a steeper I-V characteristics of the form $I \alpha V^{2.6}$ occurs over a current range of about two orders of magnitude.

Fig. 17 shows the I-V characteristics of the same sample at other temperatures. Comparing the characteristics at 270°K with those at 298°K, we see that the steep region, $I \alpha V^{2.6}$, is strongly temperature dependent. We will show later that this temperature-dependence, is not related to the increase of thermally excited carriers, which are responsible for the temperature dependence in the low-voltage ohmic region.

Because of limited power dissipation, the steep region cannot be reached at higher temperatures (Fig. 17). This is rather unfortunate as more information could have been revealed had this been permissible.

Another interesting plot is given in Fig. 18 which shows the forward conductance I/V in the ohmic regime of the I-V characteristics with respect to the reciprocal of absolute temperature 1/T. This plot shows, within the temperature range shown, the conductivity has the usual behavior,

$$\frac{I}{V} \alpha \exp \left(- \frac{E_a}{kT}\right),$$

with activation energy $E_a = 0.58$ ev.

This, together with the strong thickness dependence of current in the $I \alpha V^{2.6}$ region shown later, suggests that, within the temperature range shown and throughout

Fig. 17. The forward I-V characteristics of vacuum-annealed sample SD-10 at various temperatures. (Both axes are on a logarithmic scale.)

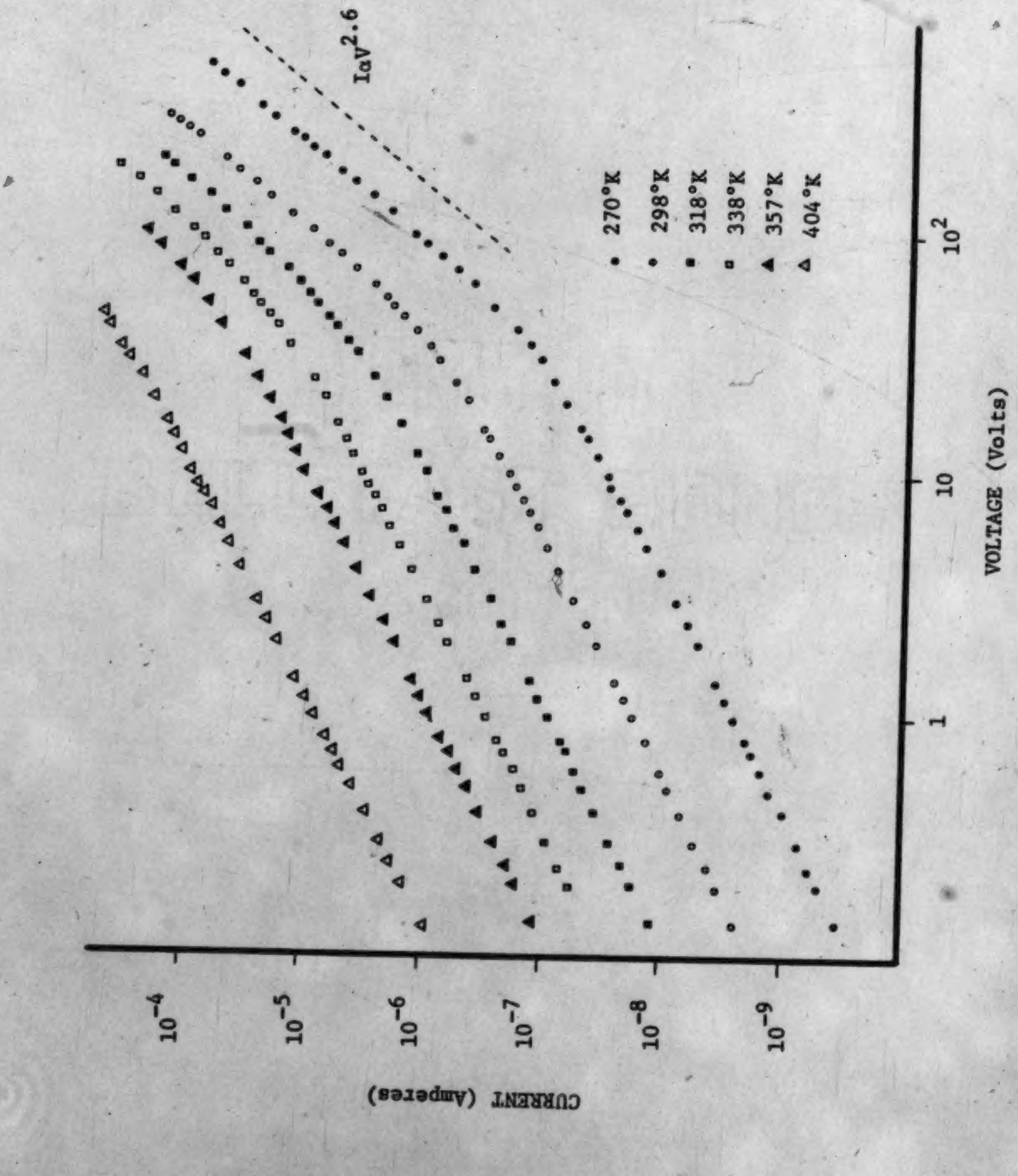
IαV$^{2.6}$
● 270°K
○ 298°K
■ 318°K
□ 338°K
▲ 357°K
△ 404°K
CURRENT (Amperes)
10^{-4}
10^{-5}
10^{-6}
10^{-7}
10^{-8}
10^{-9}
VOLTAGE (Volts)
1
10
10^{2}

Fig. 18. The forward conductance of sample SD-10 versus the reciprocal of absolute temperature. (The vertical axis is on a logarithmic scale.)

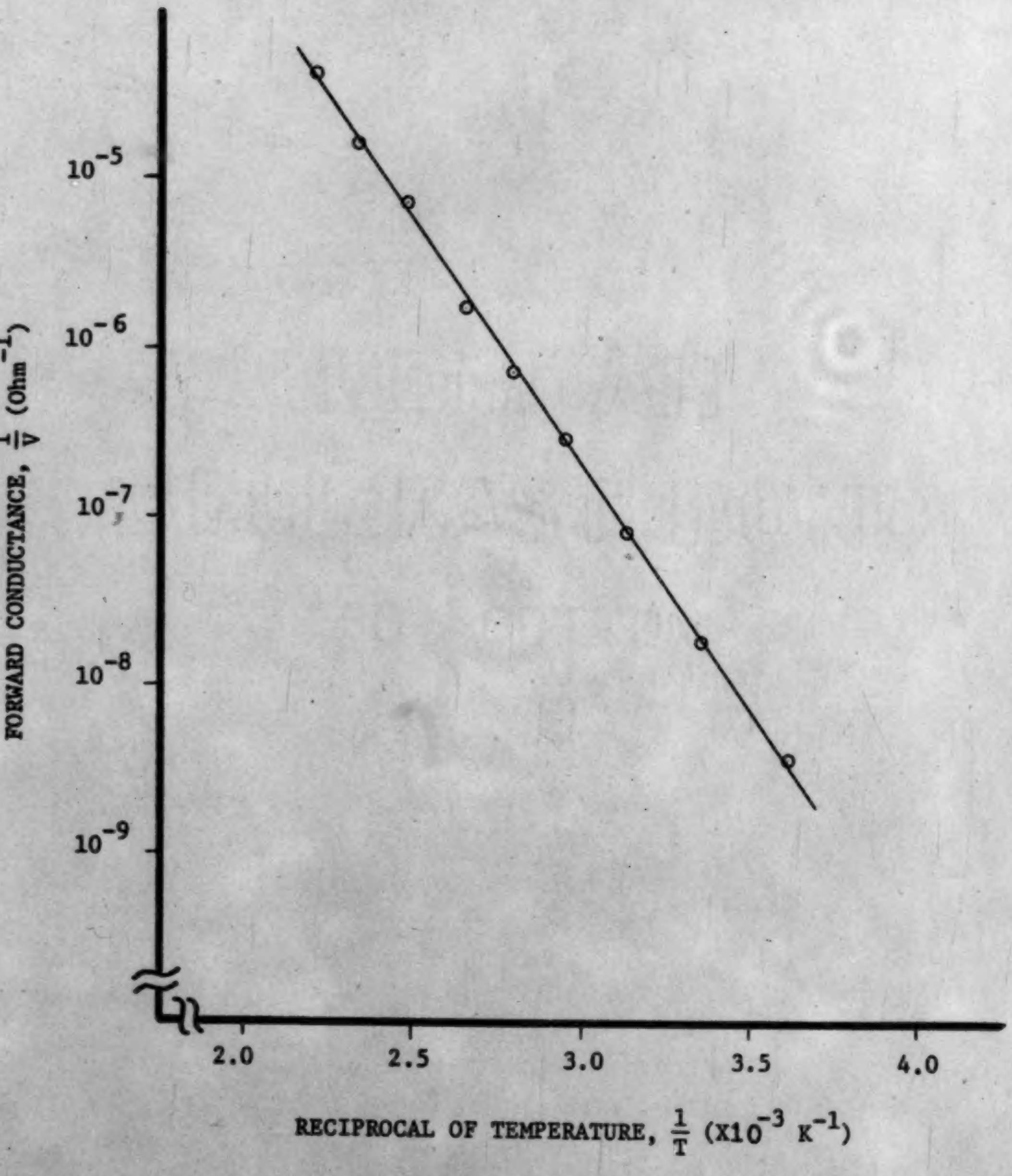
FORWARD CONDUCTANCE, $\frac{I}{V}$ (Ohm^{-1})
10^{-5}
10^{-6}
10^{-7}
10^{-8}
10^{-9}
2.0
2.5
3.0
3.5
4.0
RECIPROCAL OF TEMPERATURE, $\frac{1}{T}$ (X10^{-3} K^{-1})

the voltage range accessible, a well-behaved bulk region is responsible for the I-V characteristics observed. The voltage drops across the Pt-Cu_2O contact and the Cu_2O-Cu junction are negligible. This is, of course, supported by the presence of a well-behaved ohmic region at low voltages.

3.3 Current-thickness relation:

Although a power relation in the current-voltage characteristics over a considerable range of currents is a good indication of injection regimes, a study of current-thickness relation at a fixed voltage is necessary if the interpretation is to be unambiguous.

As shown by Lampert and Mark (1970), the I-V characteristics in the injection regime have the general form,

$$\frac{J}{L} = f\left(\frac{V}{L^2}\right) \qquad (4\text{-}28)$$

if the carrier mobility is independent of the applied field. The function f(x) depends, of course, on the type of localized states involved as we discussed in section 2 of this chapter. The relation (4-28) is the universal scaling law for injection regimes. A distinctive feature of relation (4-28) is the current and thickness relation which is very different from that caused by other effects.

An example of relation (4-28) is equation (4-26) where we have,

$$J \,\alpha\, \frac{V^{\ell+1}}{L^{2\ell+1}} \tag{4-29}$$

which can, of course, be written as,

$$\frac{J}{L} \,\alpha\, \left(\frac{V}{L^2}\right)^{\ell+1} \tag{4-30}$$

which agrees with (4-28).

As shown in Fig. 16, the current and voltage has the relation $I \alpha V^{2.6}$, i.e. with $\ell = 1.6$. Thus, from (4-29), the current-thickness relation at constant voltages in that regime would be,

$$J \,\alpha\, \frac{1}{L^{4.2}}$$

Thickness tests have been carried out in sample SD-10. The thickness is reduced by repeatedly etching in dilute HNO_3. Fig. 19 shows the results. The current density shown corresponds to an applied voltage of 300 volts, which is inside the $I \alpha V^{2.6}$ regime. A least square fit for the data gives a slope of 4.0 which is rather close to the predicted value of 4.2.

3.4 The photomemory effect and the forward I-V characteristics of vacuum-annealed diodes:

Cu_2O has long been known to exhibit a photomemory effect (Kuzel 1961, Zouaghi et. al. 1970, Tapiero et. al. 1976). This effect involves the enhancement of dark

Fig. 19. The current at 300 volts versus the thickness of the Cu_2O single crystal (vacuum-annealed sample). Both axes are on a logarithmic scale.

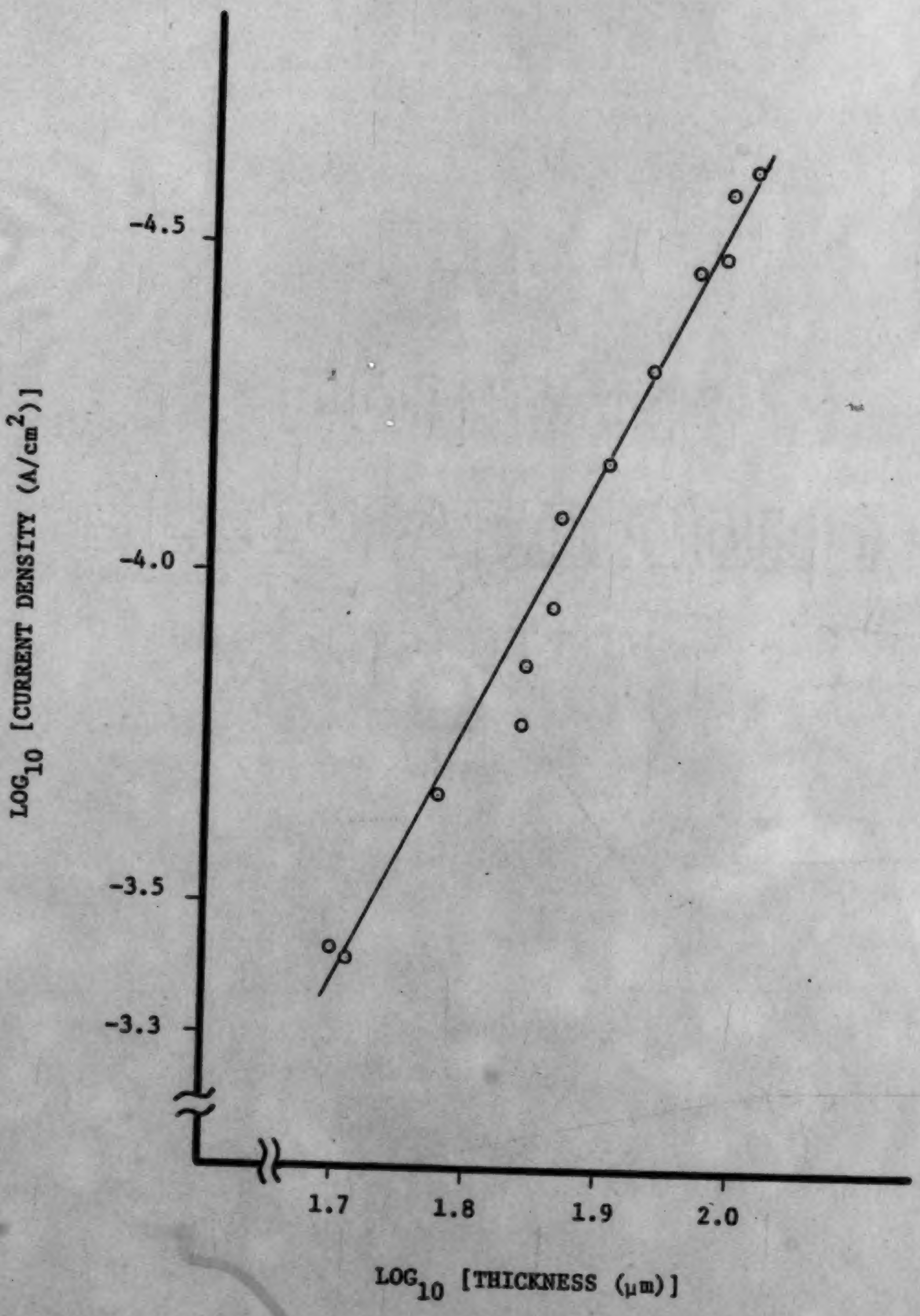
-4.5
-4.0
-3.5
-3.3
LOG$_{10}$ [CURRENT DENSITY (A/cm^2)]
1.7
1.8
1.9
2.0
LOG$_{10}$ [THICKNESS (μm)]

conductivity of a Cu_2O crystal after exposure to light. The enhancement is especially prominent in high resistivity crystals. Kuzel (1961) demonstrated that the photomemory effect is a bulk rather than surface effect, and Zouaghi et. al. (1970) further showed that the enhancement in conductivity is due mainly to the increase in the density of free holes, although the hole mobility is also slightly affected.

Recently, the results of Tapiero et. al. (1976) indicated that the increase of free holes can be caused by the trapping of photoelectrons by some deep electron traps. During the optical excitation process, electrons are excited from the valence band or from ionized centers to the conduction band and are subsequently captured by the deep electron traps. If the temperature is sufficiently low, the electrons will stay in the traps even after the light is removed. A pseudo-equilibrium will be established in the valence band-acceptor system and more free holes are created.

As we have discussed in section 3.2, the Cu_2O single-crystal bulk region is responsible for the forward I-V characteristics of the diodes. The dark current in the low-voltage ohmic regime of the forward I-V characteristics is therefore expected to be affected by the photomemory effect. An example showing the effect of exposure to light on the dark forward current is shown in Fig. 20,

Fig. 20. Dark current versus time of light exposure (photo-memory effect), at 10 volts.
Curve (1) corresponds to a light intensity of 60 watt light bulb at 8 inches distance.
Curve (2) corresponds to a light intensity of 60 watt light bulb at 4 inches distance.
(Sample SD-5)

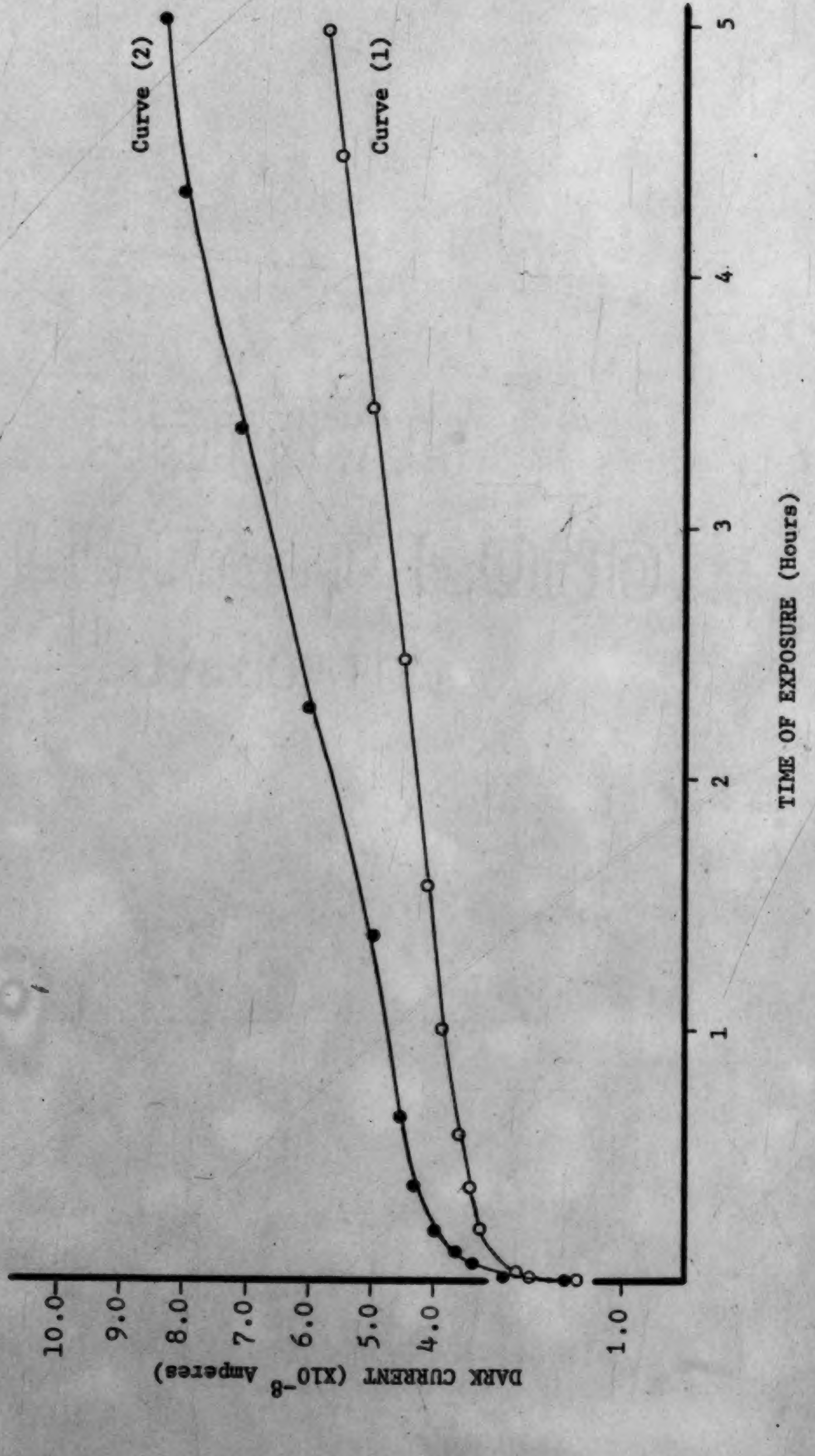
Curve (2)
Curve (1)
DARK CURRENT (X10^{-8} Amperes)
10.0
9.0
8.0
7.0
6.0
5.0
4.0
1.0
TIME OF EXPOSURE (Hours)
1
2
3
4
5

where the dark current is plotted against cumulative exposure time. The current reading was taken approximately half an hour after the light had been switched off. Curve (1) corresponds to a light intensity of a 60 watt light bulb at 8 inches distance and is less than that of curve (2) (the same light bulb at 4 inches distance). As shown in the figure, the enhancement of the conductivity still proceeds even after 5 hours of light exposure, although the rate of enhancement does slow down.

As mentioned above, the results by Zouaghi et. al. (1970) show that the density of holes, p_o', can be increased by the exposure to light. This method of increasing the density of holes, p_o', is useful because it is not accompanied by a change in lattice temperature.

We have used this method to increase the density of holes, p_o', and studied the variation in I-V characteristics due to this increase. If single-injection SCL conduction is the mechanism involved, the increase of p_o' would increase the ohmic current and extend the ohmic region to higher voltages, but the $I \alpha V^{2.6}$ regimes of the curves taken after different light exposures should merge. This is clearly supported by the experimental results shown in Fig. 21. The lowest curve (points ●) corresponds to the I-V characteristics after the sample has been preheated to about 200°C to erase any previous photomemory. The erasure of photomemory by heating is more clearly

Fig. 21. The forward I-V characteristics of vacuum-annealed sample SD-10 at temperature 273°K.

● data taken after the sample had been preheated to 200°C to erase any previous photomemory.

○ Δ ■ } data taken after the sample had been exposed to light in increasing order of total flux.

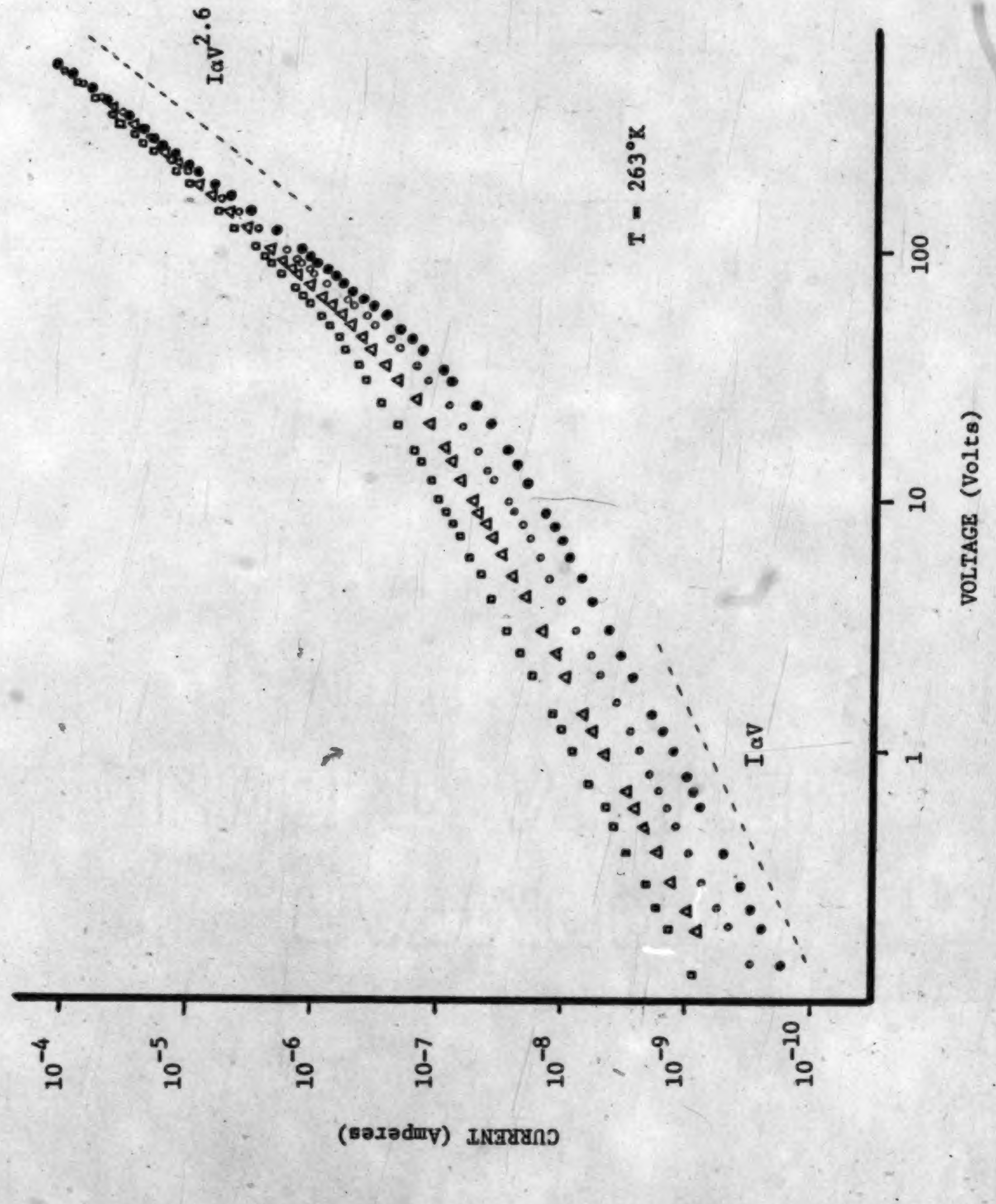
CURRENT (Amperes)
10^-4
10^-5
10^-6
10^-7
10^-8
10^-9
10^-10
VOLTAGE (Volts)
1
10
100
IαV^2.6
IαV
T = 263°K

shown in Fig. 6 of chapter 2. The three upper curves (points o, Δ, ● respectively) in Fig. 21 correspond to the dark I-V characteristics after the sample has been exposed to light. The increase of the conductivity is obvious in the ohmic region. The $I \alpha V^{2.6}$ regimes in various curves merges at higher voltages.

This experiment clearly demonstrates that the carriers that dominate the ohmic conduction regime play little role in the conduction mechanism in the $I \alpha V^{2.6}$ regimes. This is consistent with the concept of one-carrier SCL conduction since conduction in this regime is dominated by the injected carriers, rather than the thermally excited carriers which are responsible for the ohmic regime.

3.5 The transient current response to a voltage step:

The DC measurement of I-V characteristics and the thickness test described above have proven that excess carrier injection is the cause for higher power relation between current and voltage observed in the vacuum-annealed samples. We shall briefly give here another piece of experimental evidence, regarding the transient current response to a voltage step, to support this interpretation.

Instead of the DC power supply used in the DC measurement, a Velonex high power pulse generator (model 350) is used to supply square pulses across the sample and the series resistance. Fig. 22 shows the oscillogram of

Fig. 22. The transient current response to a voltage step.
Upper trace: square voltage pulse
scale: horizontal 10 μsec/cm.
vertical 100 V/cm.
Lower trace: current response
scale: horizontal 10 μsec/cm
vertical 5×10^{-4} A/cm

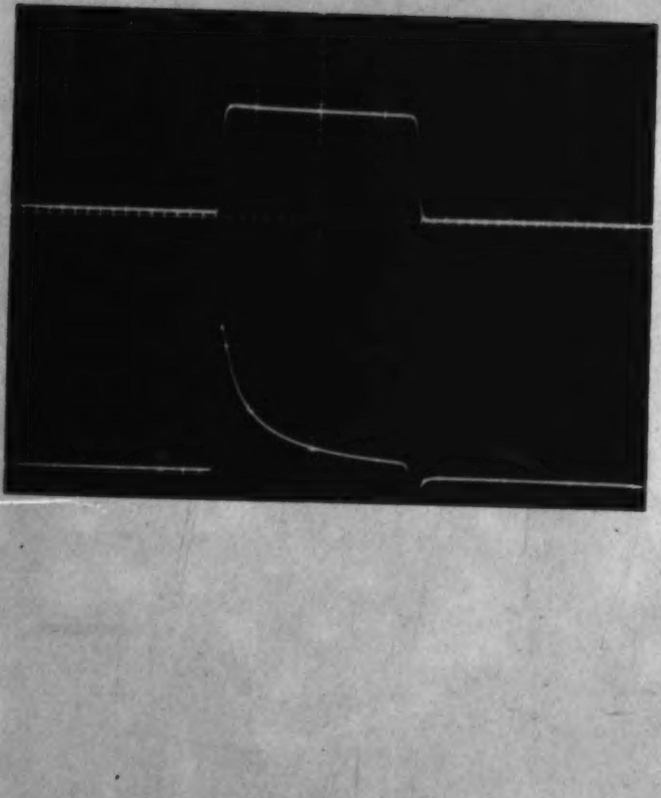

the input voltage pulse (top) and the corresponding current response (bottom). The height of the pulse (170 volts) is chosen to be large enough to bias the sample in the $I \alpha V^{2.6}$ regime in DC measurement. As shown in Fig. 22, at the on-set of the pulse, a sharp initial increase of current is observed, followed by a decay.

The current response is typical of that of single-carrier SCL diodes (Lemke 1966, Lemke and Muller 1967). The current decay is caused by trapping of injected carriers. We shall not go into the analysis of transient response in greater detail, but quote a theoretical result by Lemke (1966) in Fig. 23 for the purpose of comparison.

This experiment serves to establish that single-carrier injection, rather than double injection, is responsible for the power relation observed in I-V characteristics. In the case of double injection, the transient response is quite different from what we observed. The transient response in double injection diodes have been discussed by Baron et. al. (1966), Marsh and Viswanathan (1967), Dean (1968, 1969) and Baron and Mayer (1970). It was found that, in that case, after the on-set of the voltage step, a rise in current to its steady-state value is observed rather than a decay in current as in the case of single carrier injection with trapping.

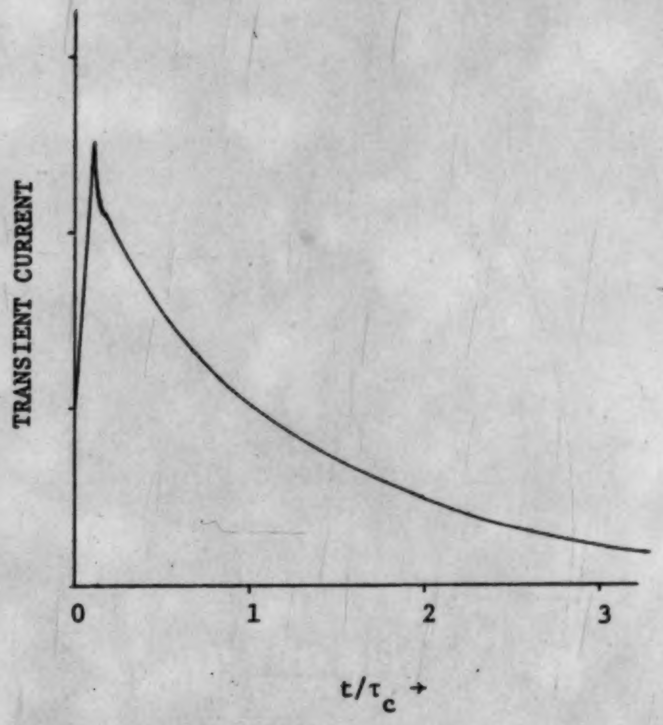

Fig. 23. Transient current for single-carrier SCL diode in response to a voltage step, with trap present.

τ_c = trapping time

(theoretical, after Lemke 1966)

(4) Conclusion for chapter 4:

In this chapter, we have shown that the various experimental results all indicate that the I-V characteristics of the vacuum-annealed samples are those of single-carrier SCL conduction. The results also indicate that a continuous distribution of localized states exist in the bulk.

The existence of the continuous localized states in Cu_2O crystals agrees with the suggestion made by Noguet et. al. in an attempt to explain the wide variation of activation energies of Cu_2O and other experimental results in optical absorption experiments.

Chapter 5

Cu_2O-Cu Double Injection Diodes

(1) Introduction

In chapter 4, we have reported the results on vacuum-annealed samples. Their forward I-V characteristics exhibit power relations. The results of various experiments showed that they are single injection diodes.

A different set of samples which were annealed at higher air pressure ($\approx$ 1-2 torr at 600°C for over 10 hours), shows different characteristics. The bulk material of these oxidized samples has lower resistivity ($\approx 10^6\ \Omega$-cm) than those annealed at higher vacuum. They also exhibit a power relation in the I-V characteristics. However, in addition to this, negative resistance has been observed at lower temperatures. These characteristics, together with other experimental results, indicate that double injection, i.e. injection of holes from one electrode and electrons from the other, is responsible for the behaviour of these diodes.

In the last chapter, SCL conduction due to one carrier injection was discussed in detail. In that case, only one type of carrier (either holes or electrons) are injected into the bulk. Therefore, every injected carrier contributes to the space charge.

However, when one of the electrodes is capable of injecting electrons, while the other is capable of injecting holes, a two carrier injection current can be observed under application of voltage with the proper polarities. Because of recombination and charge neutralization, not all injected charges contribute to the space charge. Also, since the electrons and holes are injected at opposite electrodes which are at a finite distance away from each other, the neutralization will be incomplete. However, in some cases, an assumption of quasineutrality condition can be used to simplify the solution. A variety of I-V characteristics and also some other interesting phenomena can be observed as results of double injection.

The problem of double injection has been attacked (Lampert 1959, Lampert and Rose 1961, Lampert 1962, Lampert and Mark 1970, Baron and Mayer 1970) using various approximations. In the following sections, we shall first give a brief discussion on the general theoretical approach of the problem of double injection. The case of semiconductors with large numbers of deep recombination centers is then reviewed. After that, the experimental results on Cu_2O diodes are compared with the theoretical results.

(2) General theoretical approach to double injection

The starting equations for treating the double injection problem are those which apply to all problems of current flow in semiconductors and insulators. They are,

The Poisson's equation:

$$\frac{\varepsilon}{e}\frac{dE}{dx} = \delta p - \delta n - \delta n_R \qquad (5\text{-}1)$$

where E is the electric field, δn, δp the densities of the excess injected electrons and holes respectively, while δn_R is the change in the density of electrons occupying recombination centers under injection condition as compared to the density at thermal equilibrium, x is the distance inside the crystal (taking x = 0 at the anode), and ε the dielectric constant of the crystal.

The continuity equations:

$$\frac{1}{e}\frac{dJ_n}{dx} = r \qquad (5\text{-}2a)$$

$$-\frac{1}{e}\frac{dJ_p}{dx} = r \qquad (5\text{-}2b)$$

where J_n, J_p are the electron and hole current densities respectively, and r the rate of recombination.

And finally the current flow equations,

$$J_n = e\mu_n \left[n\,E + \frac{kT}{e}\frac{dn}{dx}\right] \qquad (5\text{-}3a)$$

$$J_p = e\mu_p \left[pE - \frac{kT}{e}\frac{dp}{dx}\right] \qquad (5\text{-}3b)$$

$$J = J_n + J_p \tag{5-3c}$$

where μ_n, μ_p are the mobilities of electrons and holes respectively, n, p the total densities of electrons and holes respectively (i.e. $n = n_o + \delta n$, $p = p_o + \delta p$), and J the total current density.

For a specific problem, the appropriate boundary conditions must, of course, be included. In general, two boundary conditions are required to solve (5-1) to (5-3). In the case of double injection, because of some approximations adopted to simplify the problem, (5-1) to (5-3) are reduced to solving a first order differential equation and thus only one boundary condition can be imposed. This will be discussed later.

Furthermore, the manner of recombination will also affect the solution. Recombination can take place through localized recombination centers or accomplished directly by band to band transitions. For wide band gap semiconductors, such as Cu_2O, recombination through localized recombination centers are usually the dominant mechanism. A derivation of the rate of recombination for this mechanism is given in Appendix B.

(3) Double injection in insulators or semiconductors with a large density of deep centers:

We will consider the case of a p-type semiconductor with a large density of deep recombination centers as shown in Fig. 24. The centers are assumed to be acceptor-like, i.e. they are negatively charged when occupied by electrons and neutral when empty. The state E_R is assumed to be well below the Fermi level $E_{F,o}$ at thermal equilibrium, i.e. $E_{F,o} - E_R >> kT$. As a result, the centers are mostly occupied by electrons at thermal equilibrium, i.e. $n_{R,o} >> p_{R,o}$, where $n_{R,o}$ is the density of charged centers and $p_{R,o}$ the density of neutral centers at thermal equilibrium.

At very low voltages, the current is mainly carried by thermally excited holes in the crystal. The conduction is therefore ohmic in character.

As the voltage is increased, more carriers are injected. Deviation from ohmic behaviour occurs when the injected carriers dominate the conduction. A number of regimes can occur depending on the injection level.

Since the acceptor-like hole traps are negatively charged when occupied by electrons, the capture cross section for holes σ_p in charged centers is greater than the capture cross section for electrons σ_n on neutral centers, i.e. $\sigma_p > \sigma_n$. Also since $n_{R,o} >> p_{R,o}$, at low voltages the electron lifetime, given by $\tau_{n,o} = \frac{1}{<c_n>p_{R,o}}$, is greater than the hole lifetime, given by $\tau_{p,o} = \frac{1}{<c_p>n_{R,o}}$,

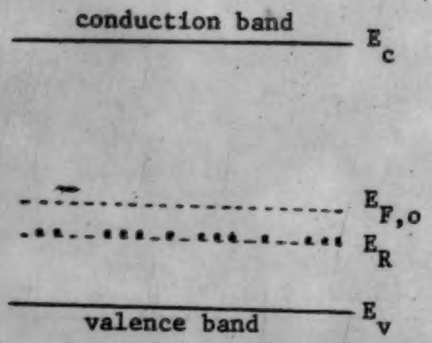
conduction band
E_c
$E_{F,o}$
E_R
valence band
E_v

Fig. 24. Schematic energy-band diagram for a semiconductor, with partially filled recombination centers, at thermal equilibrium.

where $\langle c_n \rangle$, $\langle c_p \rangle$ are defined in Appendix B. As a consequence, the injected holes are mostly trapped near the vicinity of the anode. The current is then mainly carried by the injected electrons at low injection level.

Let us begin at very low injection level, when the change in the density of ionized centers, $|\delta n_R|$, are negligible compared to the ionized centers at thermal equilibrium, $n_{R,o}$, or neutral centers, $p_{R,o}$. That is, we have

$$n_{R,o} >> p_{R,o} >> |\delta n_R| .$$

The rate of recombination, as derived in Appendix B, is given by (B-17) and (B-18), i.e.

$$r = [\delta p \; n_{R,o} + (p_o + \delta p + p_1) \; \delta n_R] \; \langle c_p \rangle \qquad \text{(B-17)}$$

and
$$r = [\delta n \; p_{R,o} - (n_o + \delta n + n_1) \; \delta n_R] \; \langle c_n \rangle \qquad \text{(B-18)}$$

Adopting the condition $n_{R,o} >> p_{R,o} >> |\delta n_R|$, (B-17) and (B-18) can be simplified as,

$$r \simeq \delta p \; n_{R,o} \cdot \langle c_p \rangle \qquad \text{(5-4)}$$

and,
$$r \simeq \delta n \; p_{R,o} \cdot \langle c_n \rangle \simeq n \; p_{R,o} \cdot \langle c_n \rangle \qquad \text{(5-5)}$$

where we have ignored n_o in the above equation since we are dealing with a p-type semiconductor. An important implication of (5-4) and (5-5) is that the lifetimes of the holes and electrons in this regime are essentially constant and equal to the values at thermal equilibrium, that is,

$$\tau_p \simeq \tau_{p,o} = \frac{1}{\langle c_p \rangle n_{R,o}}$$

and
$$\tau_n \simeq \tau_{n,p} = \frac{1}{\langle c_n \rangle p_{R,o}}.$$

As the voltage is increased further, the injection level increases. A new regime with $n_{R,o} >> |\delta n_R| >> p_{R,o}$, will be reached. At this stage, the rate of recombination is given by,

$$r \simeq \delta p \; n_{R,o} \langle c_p \rangle \qquad (5\text{-}7)$$

$$r \simeq - \delta n \; \delta n_R \langle c_n \rangle \simeq - n \delta n_R \langle c_n \rangle \qquad (5\text{-}8)$$

from equation (B-17) and (B-18) in Appendix B (note that δn_R is a negative quantity). An important result from (5-7) is that the hole lifetime remains constant and equal to the thermal equilibrium value, that is,

$$\tau_p \simeq \tau_{p,o} = \frac{1}{\langle c_p \rangle n_{R,o}} .$$

However, relation (5-8) indicates that the electron lifetime is no longer a constant but decreases as the rate of injection increases. The electron lifetime at this stage is given by,

$$\tau_n = \frac{1}{(-\delta n_R) \langle c_n \rangle} \qquad (5\text{-}9)$$

The quantity $(-\delta n_R)$ increases as injection level increases and τ_n decreases accordingly.

We shall refer later to the above two regimes as the low level regime. An essential characteristic of these two regimes is that, because of $\sigma_p >> \sigma_n$ and $n_{R,o} >> p_{R,o}$, the injected holes are mostly trapped near the anode. As a consequence, the current is mainly carried by the injected electrons. The analysis of these regimes are relatively simple and will be given in further detail in the next section.

However, as the injection level is increased further, holes begin to take a role in conduction. More centers are emptied because of the capture of injected holes. As a result, injected holes begin to be able to traverse the crystal. In other words, the lifetime of the holes increases. The analysis of this regime is rather difficult without further approximations. The method of regional approximation used by Lampert and Mark (1970) proved to be very powerful in analysing the problem. We shall follow this analysis in greater detail later.

First, to get a rough idea of what happens in this high injection level regime, we note that the larger the density of injected holes, the easier the holes can traverse the crystal. In fact it can be so much easier that the voltage required across the crystal decreases as the current increases, resulting in a striking phenomenon known as the negative resistance.

At an even higher injection level, the lifetimes of electrons and holes approach a common value. This is the so called injected plasma condition. This is the regime where the centers are completely neutral. All the electrons are transferred from the charged centers to the conduction band. The change of hole lifetime from low injection level to the injected plasma condition can be several orders of magnitude.

In the next section, we shall discuss the low injection regimes and compare the experimental results on Cu_2O diodes with the theoretical results. The analysis on the high injection regime are then discussed in section 5 of this chapter using Lampert's regional approximation. Experimental results on negative resistance in Cu_2O diodes will also be given.

(4) Low injection level:

4.1 Theory:

As mentioned in the last section, there are several regimes that can occur at low injection levels beyond the ohmic region. These regimes are characterized by the fact that most of the injected holes are captured in the vicinity of the anode because $\sigma_p >> \sigma_n$ and $n_{R,o} >> p_{R,o}$. The current is then mainly due to injected electrons. This leads to simplified current flow equations, given as,

$$J_n \simeq e\mu_n nE \qquad (5\text{-}10)$$

$$J_p \simeq e\mu_p p_o E \qquad (5\text{-}11)$$

$$J \simeq J_n \simeq e\mu_n nE \qquad (5\text{-}12)$$

The diffusion terms in (5-3a) and (5-3b) have been dropped because they are important only near the injecting electrodes. Also, in (5-12), the hole current density, J_p, is neglected compared with electron current density, J_n.

The continuity equations then give,

$$\mu_n \frac{d(nE)}{dx} = r \qquad (5\text{-}13)$$

$$-\mu_p p_o \frac{dE}{dx} = r \qquad (5\text{-}14)$$

At very low injection level, when the change in density of unoccupied centers, δp_R, is much smaller than the density of unoccupied centers at thermal equilibrium, $p_{R,o}$, the rates of recombination are given by (5-4) and (5-5) of the last section, i.e.

$$r = \delta p \; n_{R,o} \; \langle c_p \rangle \qquad (5\text{-}4)$$

and,

$$r = n \; p_{R,o} \; \langle c_n \rangle \qquad (5\text{-}5)$$

From (5-14) and (5-5), we have,

$$- \mu_p p_o \frac{dE}{dx} = n \; p_{R,o} \; \langle c_n \rangle \qquad (5\text{-}15)$$

From (5-12) and (5-15) we have,

$$- \mu_p p_o \frac{dE}{dx} = \frac{J}{e\mu_n E} \, p_{R,o} \; \langle c_n \rangle$$

or,

$$E \frac{dE}{dx} = - \frac{J}{e\mu_n\mu_p} \frac{p_{R,o}}{p_o} \langle c_n \rangle \qquad (5\text{-}16)$$

Equations (5-1) to (5-3) has been reduced to a first order differential equation. Only one boundary condition can be imposed here. This is taken as the vanishing of electric field intensity at the hole-injecting contact, that is,

$$E = 0 \text{ at } x = L \text{ (cathode)} \qquad (5\text{-}17)$$

Using (5-17) and integrating (5-16), we get,

$$\frac{E^2}{2} = \frac{J}{e\mu_p\mu_n} \frac{p_{R,o}}{p_o} \langle c_n \rangle \; (L-x)$$

$$E = \left[\frac{2J}{e\mu_p\mu_n} \frac{p_{R,o}}{p_o} \langle c_n \rangle\right]^{\frac{1}{2}} (L-x)^{\frac{1}{2}} \qquad (5\text{-}18)$$

Since, $E = - \dfrac{dV(x)}{dx}$

Thus,

$$\frac{dV(x)}{dx} = [\frac{2J}{e\mu_p\mu_n} \frac{p_{R,o}}{p_o} <c_n>]^{\frac{1}{2}} (L-x)^{\frac{1}{2}}$$

$$V(x) = \frac{2}{3} [\frac{2J}{e\mu_p\mu_n} \frac{p_{R,o}}{p_o} <c_n>]^{\frac{1}{2}} (L-x)^{3/2} \qquad (5-19)$$

$$V(L) = \frac{2}{3} [\frac{2J}{e\mu_p\mu_n} \frac{p_{R,o}}{p_o} <c_n>]^{\frac{1}{2}} L^{3/2} \qquad (5-20)$$

$$J = \frac{9}{8} e\mu_p\mu_n \frac{p_o}{p_{R,o}<c_n>} \frac{V^2}{L^3} \qquad (5-21)$$

The above $J\alpha V^2$ regime was first derived and confirmed experimentally by Ashley and Milnes (1964), and is normally known as the Ashley-Milnes regime. Equation (5-21) is derived without the use of Poisson's equation (5-1), and is purely a recombination-limited electron current.

As the injection level is increased further, a regime is reached where $n_{R,o} >> |\delta n_R| >> p_{R,o}$. The rate of recombination is given by (5-7) and (5-8) of the first section,

$$r \simeq \delta p \; n_{R,o} <c_p> \qquad (5-7)$$

To solve the J-V characteristics of this regime, Poisson's equation must be used. Baron and Mayer (1970) simplified the problem by using the quasineutrality approximation, that is, by dropping the term $\frac{\varepsilon}{e}\frac{dE}{dx}$ in Poisson's equation (5-1).

Thus,

$$\delta p - n - \delta n_R = 0 \tag{5-22}$$

The range of self-consistency of the quasineutrality approximation has been discussed by Lampert and Mark (1970).

Since in this region the density of injected holes, δp, is still quite small, we can ignore δp in (5-22). Thus,

$$n = -\delta n_R \tag{5-23}$$

Note that δn_R is a negative quantity.

From (5-8) and (5-14), we have,

$$- \mu_p p_o \frac{dE}{dx} = - n\delta n_R \langle c_n \rangle \tag{5-24}$$

From (5-23) and (5-24), we have,

$$\mu_p p_o \frac{dE}{dx} = -n^2 \langle c_n \rangle \tag{5-25}$$

Thus, we have, from (5-12) and (5-25),

$$\mu_p p_o \frac{dE}{dx} = - \left(\frac{J}{e\mu_n E}\right)^2 \langle c_n \rangle$$

$$E^2 \frac{dE}{dx} = - \frac{J^2}{e^2\mu_n{}^2} \frac{\langle c_n \rangle}{\mu_p p_o} \tag{5-26}$$

Thus,

$$E^3 = 3 \frac{J^2}{e^2\mu_n{}^2} \frac{\langle c_n \rangle}{\mu_p p_o} (L-x)$$

$$E = \left(3 \frac{J^2}{e^2\mu_n{}^2} \frac{\langle c_n \rangle}{\mu_p p_o}\right)^{1/3} (L-x)^{1/3} \tag{5-27}$$

$$\frac{dV(x)}{dx} = - \left(3 \frac{J^2}{e^2 \mu_n{}^2} \frac{\langle c_n \rangle}{\mu_p p_o}\right)^{1/3} (L-x)^{1/3}$$

$$V(x) = \frac{3}{4} \left(\frac{3J^2}{e^2 \mu_n{}^2} \frac{\langle c_n \rangle}{\mu_p p_o}\right)^{1/3} (L-x)^{4/3} \qquad (5\text{-}28)$$

$$V(0) = \frac{3}{4} \left(3 \frac{J^2}{e^2 \mu_n{}^2} \frac{\langle c_n \rangle}{\mu_p p_o}\right)^{1/3} L^{4/3}$$

$$J = \frac{8}{9} e\mu_n \left(\frac{\mu_p p_o}{\langle c_n \rangle}\right)^{\frac{1}{2}} \frac{V^{3/2}}{L^2} \qquad (5\text{-}29)$$

This regime was first derived by Baron and Mayer (1970). Unlike the Ashley-Milnes regime, this regime is derived by assuming the quasineutrality approximation. To obtain the condition under which the quasineutrality approximation holds, we have from (5-1),

$$\frac{\varepsilon}{e} \frac{dE}{dx} \approx - n - \delta n_R \qquad (5\text{-}30)$$

(5-24) and (5-30) then give,

$$- \frac{e\mu_p}{\varepsilon} p_o = \frac{-n\delta n_R \langle c_n \rangle}{-n-\delta n_R}$$

or,

$$n \left(\delta n_R \langle c_n \rangle + \frac{e\mu_p p_o}{\varepsilon}\right) = - \frac{e\mu_p p_o}{\varepsilon} \delta n_R \qquad (5\text{-}31)$$

Comparing (5-23) with (5-31), we can see the quasineutrality approximation will hold only if,

$$|\delta n_R| \langle c_n \rangle << \frac{e\mu_p p_o}{\varepsilon}$$

or,

$$|\delta n_R| << \frac{e\mu_p p_o}{\varepsilon \langle c_n \rangle} \qquad (5\text{-}32)$$

Since the resistivity of the crystal, ρ, is given by,

$$\rho = \frac{1}{e\mu_p p_o}$$

and since the electron lifetime at thermal equilibrium is given by,

$$\tau_{n,o} = \frac{1}{<c_n> n_{R,o}} ,$$

we have,

$$|\delta n_R| << \frac{\tau_{n,o}\, n_{R,o}}{\rho\epsilon}$$

or

$$\frac{|\delta n_R|}{n_{R,o}} << \frac{\tau_{n,o}}{t_{ohm}} \qquad (5\text{-}33)$$

where $t_{ohm} = \rho\epsilon$ is the ohmic relaxation time of the crystal. Relation (5-33) indicates that the higher the ratios $\frac{p_o}{n_{R,o}}$, the wider the range over which the quasineutrality approximation holds.

We must mention here that, in practice, not all the regimes discussed above occur. Depending on the actual parameters of the crystal concerned, some regimes can be entirely missing or too short to be identified as a distinct regime.

Furthermore, the relation between I and V alone cannot unambiguously establish which regime is involved. For example, if one of the mobilities (μ_n or μ_p) becomes field dependent in the form $\mu \; \alpha \; E^{-\frac{1}{2}}$, the Ashley-Milnes regime can have the I-V relation of the form $I \alpha V^{3/2}$, which has the same functional relation as that in the Baron-Mayer regime. Further information is necessary to establish the correct regime involved. In this case, the two regimes can be distinguished from one another by a study of the relation between J and p_o. The Ashley-Milnes regimes is characterized by $J \alpha p_o$, with other parameters fixed, while Baron-Mayer regime has the form $J \alpha p_o^{1/2}$.

4.2 Experimental results on oxidized samples - low injection regime:

4.2.1 Forward I-V characteristics

As mentioned in chapter 3, annealing the diodes at higher oxygen pressure leads to a decrease in forward resistance at low voltages. For thicker samples ($\gtrsim$ 50 μm) the I-V characteristics show clear regimes. However, in thinner samples ($\lesssim$ 20 μm), the I-V characteristics exhibit the discrepancies from the ideal cases discussed above.

The DC I-V characteristics of a thick oxidized sample, SD-1 (thickness = 52 μm) is shown in Fig. 25. It shows an ohmic regime followed immediately by an $I \alpha V^{3/2}$ regime at low temperatures (e.g. at 164°K, the current in the $I \alpha V^{3/2}$ regime extends over two orders of magnitude), while at higher temperatures (e.g. room temperature), the deviations from ohmic behaviour in the voltage range accessible are quite small. As we shall show later, the $I \alpha V^{3/2}$ regime has a current-thickness relation which

__Fig. 25.__ The forward I-V characteristics of oxidized sample SD-1 at various temperatures. (Both axes are on a logarithmic scale.)

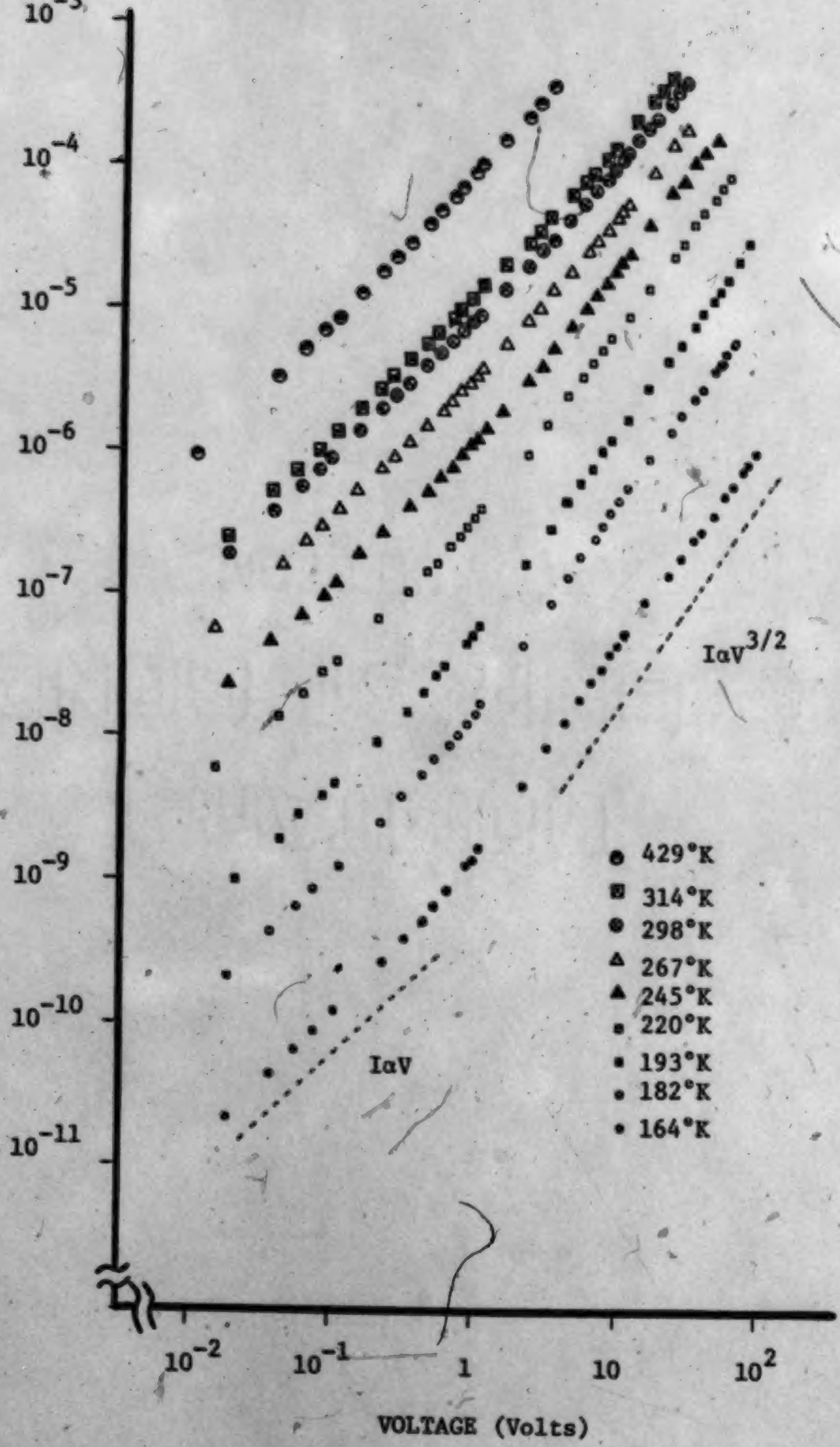
10^-3
10^-4
10^-5
10^-6
10^-7
10^-8
10^-9
10^-10
10^-11
CURRENT (Amperes)
10^-2
10^-1
1
10
10^2
VOLTAGE (Volts)
IαV
IαV^3/2
429°K
314°K
298°K
267°K
245°K
220°K
193°K
182°K
164°K

closely agrees with that expected and obeys the relation $J \alpha \mu_p p_o$. Thus, this should be the Ashley-Milnes regime with either hole or electron mobility field dependent.

The I-V characteristic of a thinner sample, SD-2, at room temperature is shown in Fig. 26. It exhibits significant deviation from ohmic behaviour even at this temperature. The low voltage ohmic region is followed by a steep region which is in turn followed by a $I \alpha V^{3/2}$ regime. The origin of the steep regime is not clear. Information on thickness-current relation in this regime was impossible to obtain since this regime occurs at very small thickness and at higher temperatures, as can be seen from Fig. 27 where the I-V characteristics at various temperatures are shown. The steep regime becomes less pronounced as temperature decreases and almost disappears at a temperature of about 226°K. Another puzzling feature of the I-V characteristics of the sample is that at lower temperatures, there is higher power relation between I and V, e.g. at 168°K (points ● in Fig. 27) a regime $I \alpha V^2$ is observed. Perhaps more exact theory including diffusion can account for the discrepancies.

4.2.2 Temperature dependence of I-V characteristics:

Since the current in the low-voltage ohmic regime is proportional to $p_o \mu_p$ at a fixed voltage, the dependence of current on this factor, $p_o \mu_p$, in the $I \alpha V^{3/2}$ regime can

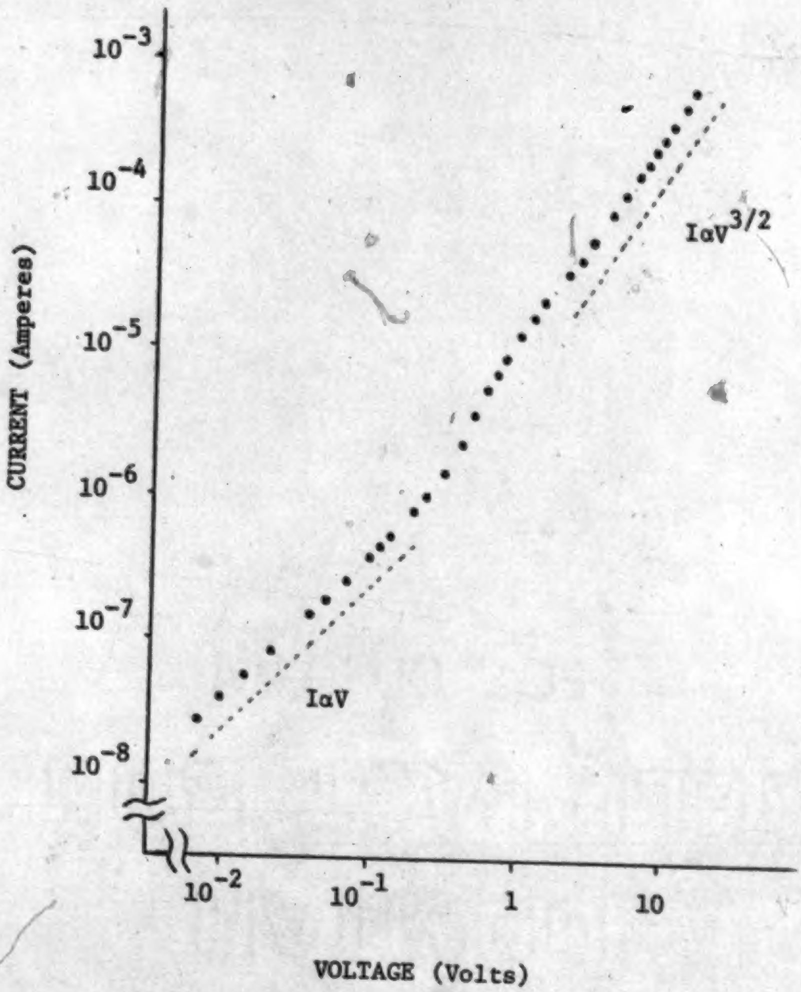

Fig. 26. The forward I-V characteristics of oxidized sample SD-2 at room temperature. (Both axes are on a logarithmic scale.)

Fig. 27. The forward I-V characteristics of oxidized sample SD-2 at various temperatures. (Both axes are in logarithmic scale.)

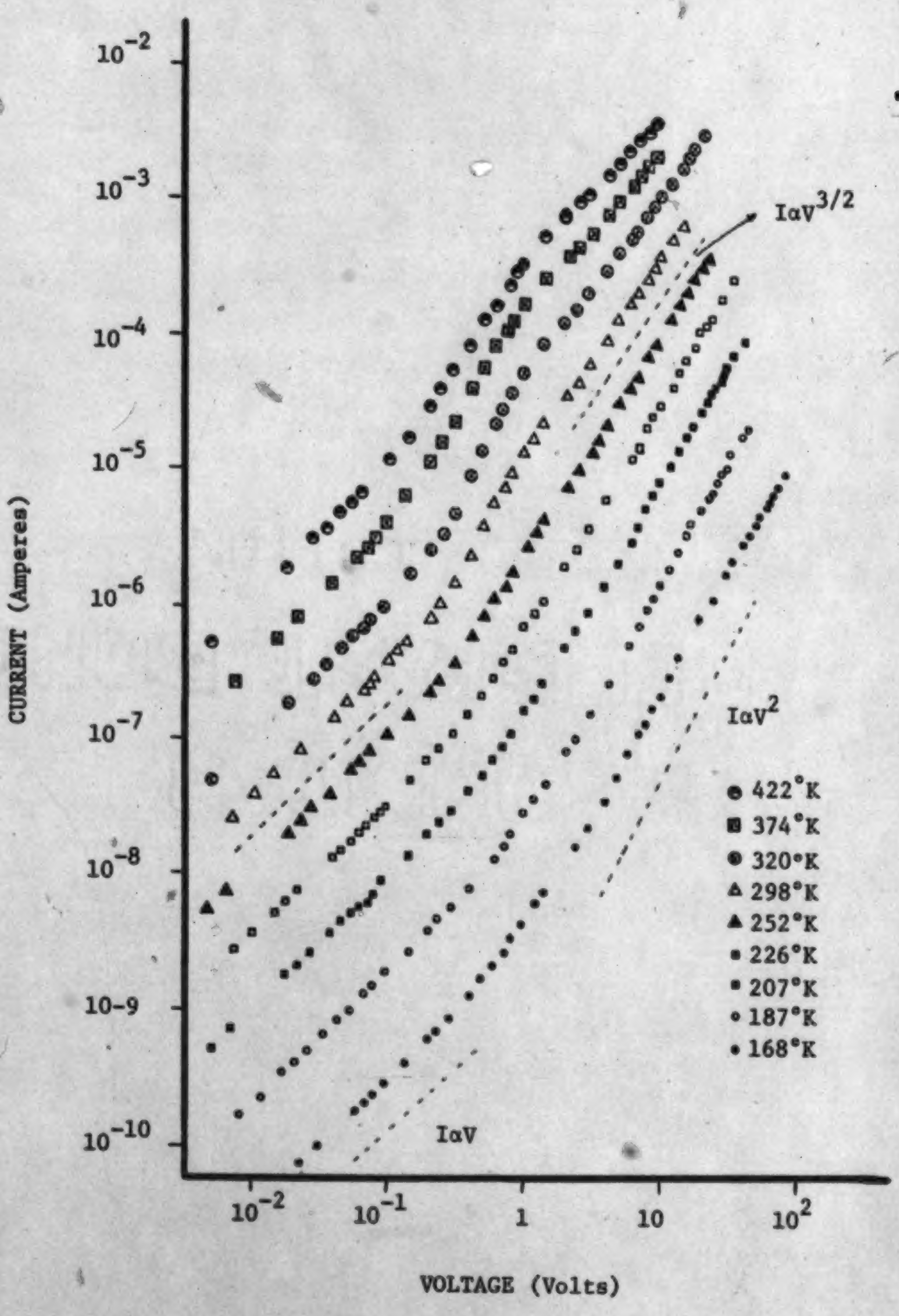
CURRENT (Amperes)
10^{-2}
10^{-3}
10^{-4}
10^{-5}
10^{-6}
10^{-7}
10^{-8}
10^{-9}
10^{-10}
$I \alpha V^{3/2}$
$I \alpha V^2$
$I \alpha V$
⊖ 422°K
⊠ 374°K
⊗ 320°K
△ 298°K
▲ 252°K
▪ 226°K
▪ 207°K
○ 187°K
• 168°K
10^{-2}
10^{-1}
1
10
10^2
VOLTAGE (Volts)

be studied by comparing the temperature dependence of currents in the two regimes. This serves as a way of determining whether the $I \alpha V^{3/2}$ regime is the Ashley-Milnes regime with field dependent mobility or the Baron-Mayer regime. The former has the relation $J \alpha \mu_p p_o$, while the later $J \alpha (\mu_p p_o)^{1/2}$.

Fig. 28 shows plots of current at 0.1 volts (ohmic regime) and the current at 10 volts ($I \alpha V^{3/2}$ regime) with the reciprocal of temperature. This indicates that both the $I \alpha V^{3/2}$ regime and ohmic regime obey the relation $J \alpha \mu_p p_o$. This, together with the thickness-current relation described below, imply that the $I \alpha V^{3/2}$ regime observed is the Ashley-Milnes regime with field dependent mobility. Note that the Baron-Mayer regime would have a $I \alpha (\mu_o p_o)^{1/2}$ dependence and the straight line of the plot I vs. 1/T in this regime would give one-half the slope of that in the ohmic regime. This is, of course, inconsistent with that shown in Fig. 28.

The slight difference in the slopes in Fig. 28 is most likely due to the temperature dependence of μ_n(refer to equation (5-21)).

The question then arises as to which mobility, μ_n or μ_p, becomes field dependent. Fortin and Weichman (1966) have reported a hole mobility up to 3000 V/cm with no sign of field dependence. It is therefore likely that it is the electron mobility that becomes field

Fig. 28. The currents in the ohmic regime and the $I \alpha V^{3/2}$ regime versus the reciprocal of absolute temperature (sample SD-1). Note that, at 0.1 volts, the sample operates in the ohmic regime, while, at 10 volts, the sample operates in the $I \alpha V^{3/2}$ regime.

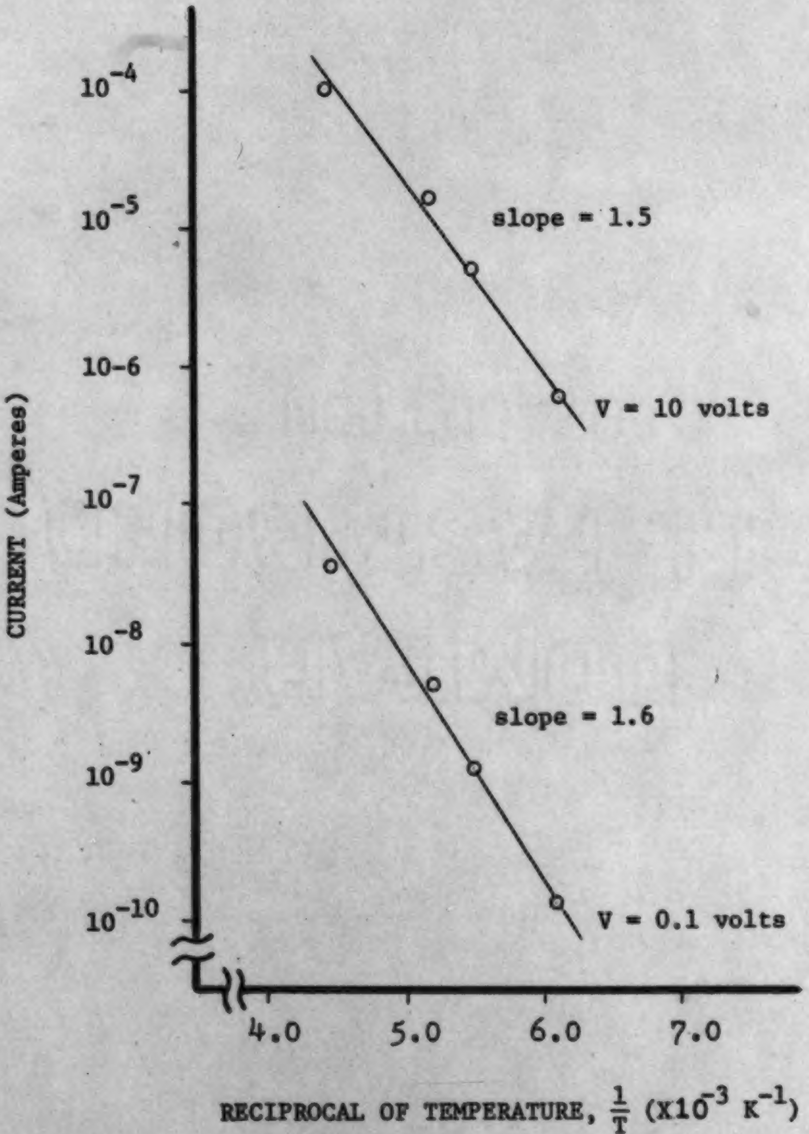

CURRENT (Amperes)
10^{-4}
10^{-5}
10-6
10^{-7}
10^{-8}
10^{-9}
10^{-10}
slope = 1.5
V = 10 volts
slope = 1.6
V = 0.1 volts
4.0
5.0
6.0
7.0
RECIPROCAL OF TEMPERATURE, $\frac{1}{T}$ ($X10^{-3}$ K^{-1})

dependent in our case. Unfortunately, the information on electron mobility in Cu_2O is rare and a comparison is not possible at this moment.

4.2.3 The effect of photomemory on the forward I-V characteristics of the oxidized samples:

As we mentioned in the previous chapter, the photomemory effect can be used as a tool to increase the hole density, p_o, (or more strictly speaking, the quantity $\mu_p p_o$ since hole mobility is also slightly affected) without changing the lattice temperature. This effect has been used to test the dependence of current on p_o in the case of vacuum-annealed samples (section 3.4 of chapter 4).

A similar experiment was carried out for sample SD-2. The sample was first preheated to about 200°C and cooled to room temperature to erase any previous photomemory. The lowest curve (curve 1) in Fig. 29 corresponds to the I-V characteristics at room temperature after preheating. The upper two curves (curves 2 and 3) correspond to behaviour after exposure to light. Unfortunately, a large increase of conductivity is not possible in the case of low resistivity sample. However, it is still possible to see from Fig. 29 that an increase in the current in the ohmic region is followed by an increase in current in the $I\alpha V^{3/2}$ regime by almost the same factor. For example,

Fig. 29. The forward current-voltage characteristic of oxidized sample SD-2 at room temperature.
o data taken after the sample has been preheated at 200°C to erase any previous photomemory.
■⎫ data taken after the sample has been exposed
•⎭ to light of increasing flux.

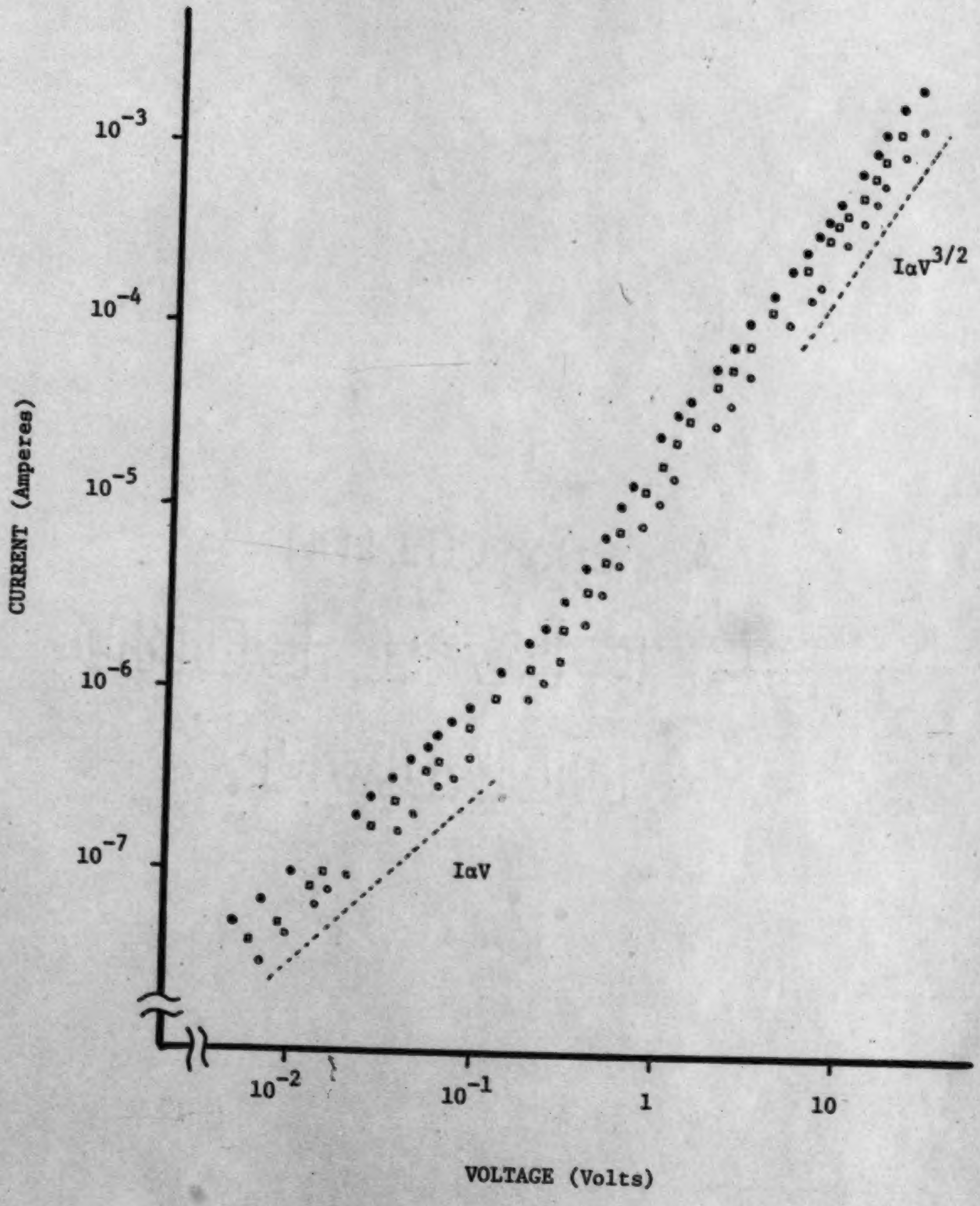
CURRENT (Amperes)
10^-3
10^-4
10^-5
10^-6
10^-7
IαV^3/2
IαV
10^-2
10^-1
1
10
VOLTAGE (Volts)

comparing curves (1) and (3), the increase in the current in the $I \alpha V^{3/2}$ regime by a factor of about two is almost the same as that in the low voltage ohmic region. This is again in agreement with the results in the previous section on the study of temperature dependence of I-V characteristics where we concluded that $I \alpha \mu_p p_o$ in the $I \alpha V^{3/2}$ regime. This in turn supports that the $I \alpha V^{3/2}$ regime is the Ashley-Milnes regime with field dependent mobility.

Note that this test also serves to rule out the possibility that the power relation of current and voltage on oxidized samples is due to single carrier injection, in which case the current in the higher power regimes would not depend on the thermal hole density, p_o.

4.2.4 The current-thickness relation in the $I \alpha V^{3/2}$ regime:

As we discussed in section 3.3 of chapter 4, the current-thickness relation is important in determining if a given regime is due to injection of carriers. As mentioned in that section, the injection regimes have the general relation,

$$\frac{J}{L} \alpha \ f\left(\frac{V}{L^2}\right)$$

for both single and double injection, with mobilities assumed to be independent of field.

For example, in the case of Ashley-Milnes regimes, we have,

$$J \alpha \frac{V^2}{L^3} \quad \text{or} \quad \frac{J}{L} \alpha (\frac{V}{L^2})^2$$

which, of course, is in the form $J/L \alpha f(V/L^2)$.

If, however, one of the mobilities becomes field dependent, in the form $\mu \alpha E^{-\frac{1}{2}}$, the $J \alpha V$ characteristics in the Ashley-Milnes regime are given as,

$$\frac{J}{L} \alpha (\frac{V}{L})^{-\frac{1}{2}} (\frac{V}{L^2})^2 = \frac{V^{3/2}}{L^{7/2}}$$

or

$$J \alpha \frac{V^{3/2}}{L^{5/2}}$$

In section 3.3 of chapter 4, we have shown the results on the current-thickness measurements on vacuum-annealed samples. A similar experiment was carried out on an oxidized sample. The thickness was again reduced by etching repeatedly in dilute HNO_3.

One more factor, however, has to be considered here. As shown in section 4.2.3, the entire I-V characteristics of an oxidized sample are affected by the photomemory effect. In the process of reducing the sample thickness by etching, the sample was inevitably exposed to light. Although the sample was preheated at 200°C every time before the I-V characteristics were taken, and thus the photomemory was largely erased, past experience has indicated that a complete return to the same resistivity state is not always obtained. For this reason, in analyzing the data, a method of normalization should be used. This is done in our case by plotting $\log_{10}(J_{3/2}/J_1)$ versus $\log_{10}L$, where $J_{3/2}$ denotes the current corresponding to a specified voltage in the $I \alpha V^{3/2}$ regime, and J_1 denotes the the current corresponding to a specified voltage in the ohmic regime, and L the thickness of the Cu_2O single crystal. Since $J_1 = e\mu_p p_o V/L$, and $J_{3/2} \alpha (\mu_p p_o) V^{3/2}/L^x$, the ratio $J_{3/2}/J_1$ should not depend on $\mu_p p_o$.

A plot of $\log_{10}(J_{3/2}/J_1)$ versus $\log_{10}L$ is given for an oxidized sample SD-6 (Fig. 30). The least square fit gives a slope of 1.2 which is in close agreement with the predicted value of 1.5.

Fig. 30. $\log_{10}(J_{3/2}/J_1)$ versus $\log_{10} L$, where $J_{3/2}$ is the current at 10 volts ($I \alpha V^{3/2}$ regime), J_1 the current at 0.1 volts (ohmic regime) and L the thickness in μm. (Sample SD-6)

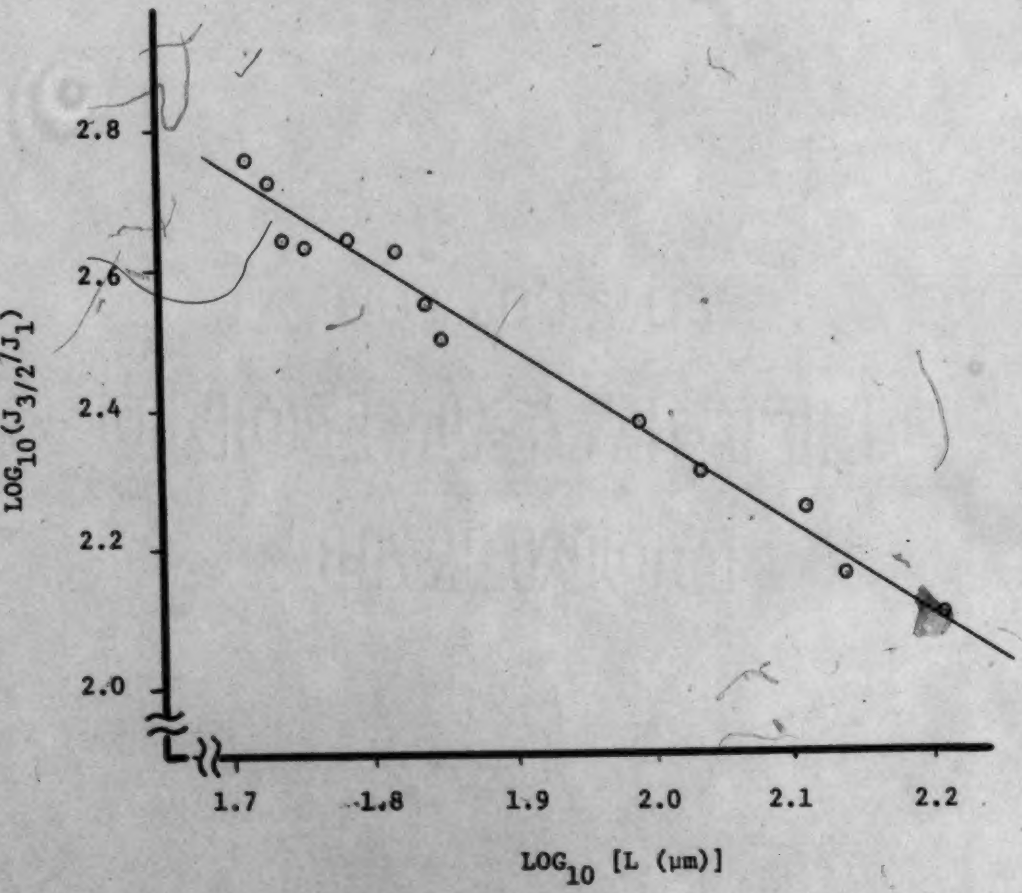

5. High injection level:

5.1 Introduction

The analysis on the low injection levels was relatively simple. The simplification was possible in that case since at low injection levels the current is mainly carried by electrons and at least one of the carrier lifetimes (hole and/or electron lifetimes remains almost constant in each regime.

The analysis on the higher injection levels is more difficult because both electrons and holes play significant roles in the conduction and the lifetimes of both carriers vary with injection level.

The regional approximation used by Lampert proved to be very powerful in analysing the high injection regime. We shall give only a brief review of the treatment of this regime by Lampert and Mark (1970). The main purpose for this review is to show how negative resistance can occur. Since quantitative comparison in the case of Cu_2O is rather difficult because many parameters for Cu_2O are not known at this stage, we intended to give only qualitative description of the experimental results on the negative resistance phenomenon.

5.2 Theory - a brief review of Lampert's regional approximation in treating the double injection problem:

In dealing with high injection levels, the densities of thermal carriers n_o, P_o are neglected. Because of the injection of electrons from the cathode and holes from the anode, we would expect the local conditions regarding the occupation of recombination centers, the amount of space charge and the densities of holes and electrons to vary continuously from anode to cathode. Lampert's regional approximation involves the splitting of the crystal into some finite number of regions where the conditions can be specified with the help of some physical arguments.

In the case shown in Fig. 24, where the recombination centers are partially filled, Lampert and Mark (1970) have attacked the problem by splitting the crystal into three regions shown in Fig. 31.

Region I: This is the region closest to the anode. Because it is adjacent to the anode where holes are injected and because $\sigma_p >> \sigma_n$, the recombination centers which were originally mostly occupied with electrons are now largely depopulated, i.e.

$$P_R \simeq N_R \qquad (5\text{-}34)$$

The electrons originally occupying this region have been transferred into the conduction band and we have,

$$n > n_{R,o} \qquad (5\text{-}35)$$

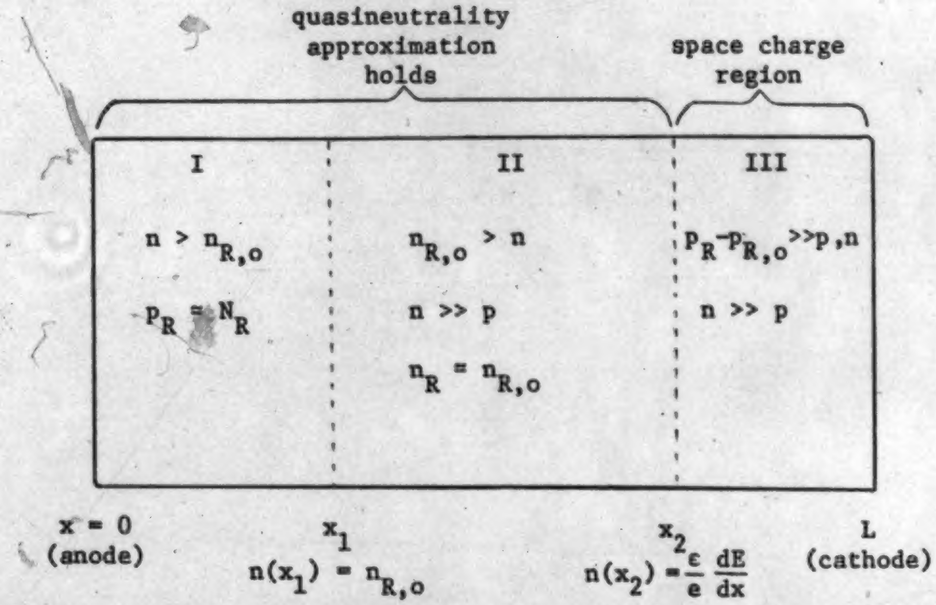
quasineutrality approximation holds
space charge region
I
II
III
$n > n_{R,o}$
$p_R = N_R$
$n_{R,o} > n$
$n >> p$
$n_R = n_{R,o}$
$p_R - p_{R,o} >> p, n$
$n >> p$
$x = 0$ (anode)
x_1
$n(x_1) = n_{R,o}$
x_2
$n(x_2) = \frac{\varepsilon}{e} \frac{dE}{dx}$
L (cathode)

Fig. 31. Schematic diagram for Lampert's regional approximation applied to the case of double injection with trapping by partially filled recombination centers.

Further, space charge is not serious and the quasineutrality condition can be used, i.e.,

$$n - p = (N_R - p_{R,o}) = n_{R,o} \tag{5-36}$$

Using (5-34), (5-35) and (5-36), the continuity equation can be written as (Lampert and Mark 1970),

$$n_{R,o}\,\frac{dE}{dx} = \frac{(a+1)n}{\mu_p \tau_{n,h}} \tag{5-37}$$

where $a = \frac{\mu_p}{\mu_n}$ and $\frac{1}{\tau_{n,h}} = \langle c_n \rangle N_R$. Also, the current flow equation can be written as,

$$J = e\mu_n E(a+1)\, n - e\mu_p\, n_{R,o} E \tag{5-38}$$

Equations (5-36), (5-37) and (5-38) together with the boundary conditions at $x = 0$ can be solved to give $E(x)$, $V(x)$ in this region.

Region II. This is the region next to region I (Fig. 31). The recombination centers are still largely filled. Thus,

$$n < n_{R,o} \tag{5-39}$$

Since most of the injected holes are captured by the recombination centers in region I, the density of free holes in this region is small compared with the density of free electrons, i.e.,

$$p \ll n \tag{5-40}$$

Again the space charge in this region is not serious, and quasineutrality conditions can be used.

Using these relations, it can be shown (Lampert and Mark 1970) that Poisson's equation, the current flow equation and the continuity equation can be simplified to give,

$$n \approx p_R - p_{R,o} = n_{R,o} - n_R \tag{5-41}$$

$$J \approx e\mu_n nE \tag{5-42}$$

$$\frac{dn}{dx} \approx - \frac{e<c_p>n^2_{R,o}}{aJN_R} n\ (n + p_{R,o}) \tag{5-43}$$

Again, equations (5-41), (5-42) and (5-43), together with the boundary condition at $x = x_1$, which is taken as $n(x_1) = n_{R,o}$, an obvious condition from (5-35) and (5-39), can be solved to give $E(x)$, $V(x)$.

Region III. This is the region closest to the cathode where the injection of electrons occurs. Since the injected holes are preferentially captured by the filled centers, the electrons dominate the conduction. Thus,

$$J \approx en\mu_n E \tag{5-44}$$

The quasineutrality approximation can no longer be used in this region. Poisson's equation gives,

$$\frac{\varepsilon}{e} \left(\frac{dE}{dx}\right) \approx p_R - p_{R,o} \tag{5-45}$$

where the terms $p-p_o$ and n are ignored.

From (5-44) and (5-45) and the continuity equations, a second order differential equation can be obtained,

$$E \frac{d^2E}{dx^2} = - \frac{e\langle c_p \rangle n_{R,o}^2 \, p_{R,o}}{\varepsilon \mu_p N_R} \qquad (5\text{-}46)$$

The voltage drop across each region can be solved from the results on E(x). The sum of the voltage drops across the three regions, of course, must be equal to the total external applied voltage across the crystal. The solution for the current-voltage characteristics have been given by Lampert and Mark (1970) and are shown in Fig. 32.

In Fig. 32, there is a threshold for current flow. A steep rise in current (A - B in Fig. 32) is followed by a negative resistance regime (B - C in Fig. 32). At very high injection level, a $J \alpha V^2$ regime appears. This is the so called semiconductor injected plasma regime.

The above results have ignored the low injection level regimes. Taking these into account, the general shape of the I-V characteristics should then look as in Fig. 33.

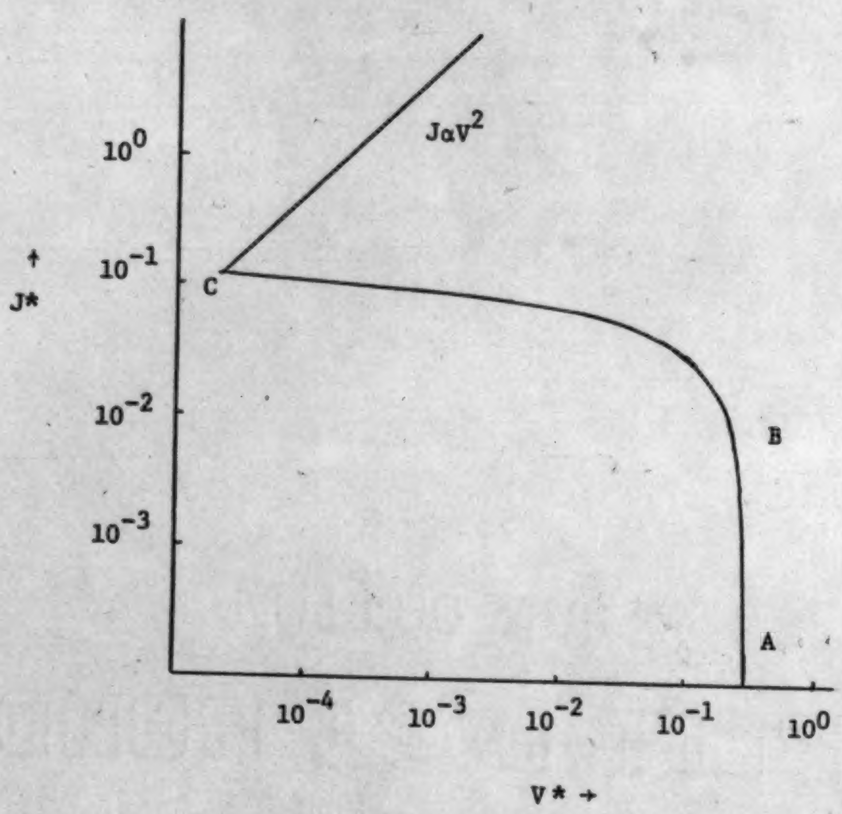

Fig. 32. Current-voltage characteristic for double injection into an insulator with a single set of recombination centers partially filled in thermal equilibrium. (Theoretical calculation, after Lampert and Mark, 1970)

J*, V* are defined as,

$$J^* = \frac{\mu_p N_R}{e<c_p>\mu_n \; n_{R,o}^2 \quad {}_{R,o}L} \tilde{J}$$

$$V^* = \frac{1}{n_{R,o}L^2} \{\frac{\varepsilon\mu_p N_R}{e\; p_{R,o}<c_p>}\}^{\frac{1}{2}} V$$

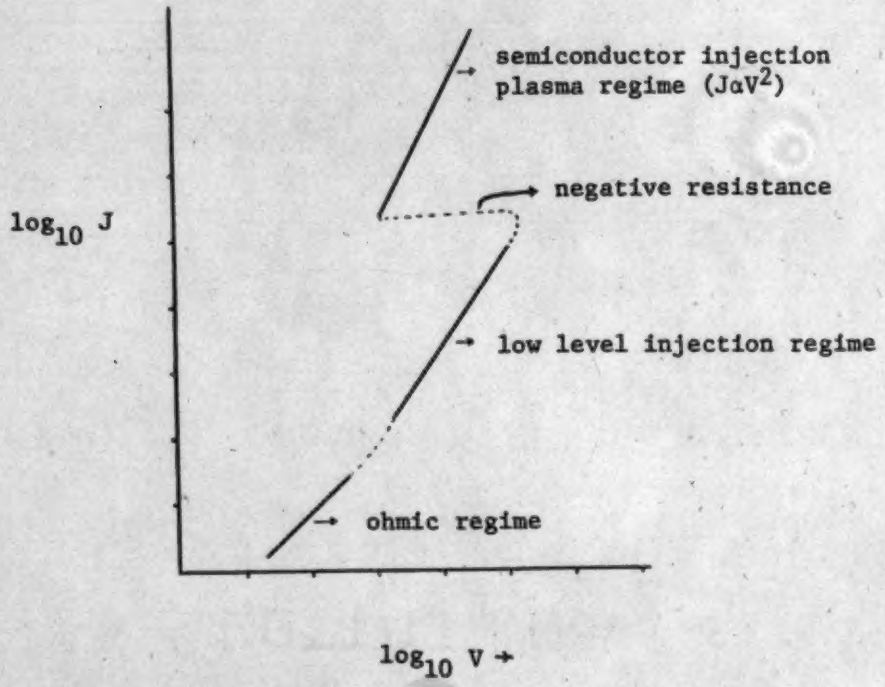

Fig. 33. A qualitative sketch of the current-voltage characteristic to be expected for double injection into an insulator with a single set of recombination centers partially filled in thermal equilibrium, including the lower-level injection regimes.

5.2 Experimental results on high injection level of oxidized samples - negative resistance:

Some preliminary results on the negative resistance phenomenon that were observed in oxidized samples will be presented in this section. Only a qualitative discussion is possible at this stage.

A typical example of negative resistance observed in the oxidized samples is shown in the oscillograms of the forward I-V characteristics of sample SD-4 at 178°K (Fig. 34). The maximum current increases for successive figures from (a) to (c). The growth of the negative resistance regime is clearly seen. A large hysterisis is observed in the negative resistance regime of the I-V characteristics. A steep portion which is believed to be due to the formation of a current filament is observed in the higher current regime of the characteristics. The slight decrease in the on-set voltage of the negative resistance in the lowest oscillagram in Fig. 34 is due to a slight increase in temperature due to the I^2R heating.

Fig. 35 (a and b) shows the I-V characteristics at higher temperatures (185°K and 183°K). The negative resistance is less pronounced, but a large hysterisis is observed.

As the temperature is raised further, the negative resistance disappears entirely. Fig. 36 shows the I-V characteristic at 236°K. The disappearance of the negative resistance is believed to be due to thermal reemission of captured holes into the valence band.

The magnitude of current that can pass through the sample is limited by power dissipation at that temperature. As a consequence, higher current regimes after the steep portion in the I-V characteristics have not been reached in our study.

Fig. 34. Oscillograms of the current-voltage characteristics of oxidized sample SD-4 at 178°K.
Scales for all three oscillograms:
horizontal axis 50 volts/cm
vertical axis 2 mA/cm
The maximum current increases for successive figures from top to bottom.

(a)

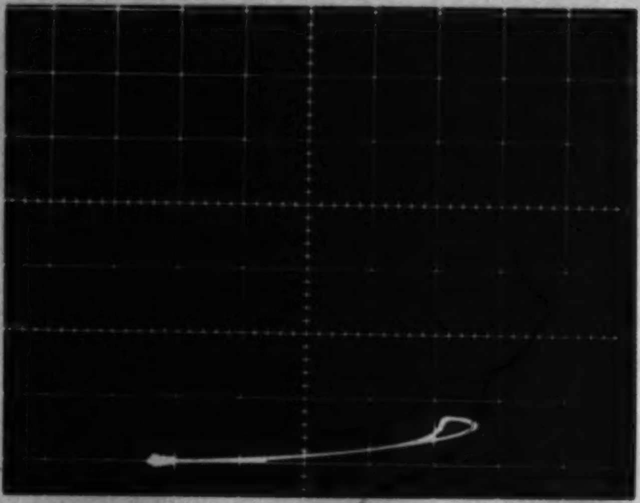

(b)

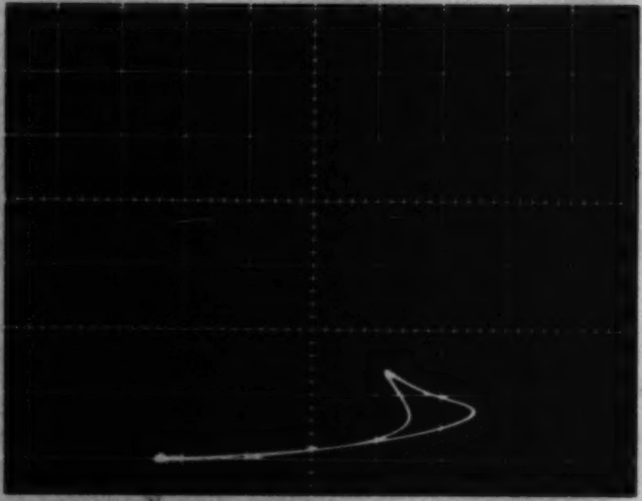

(c)

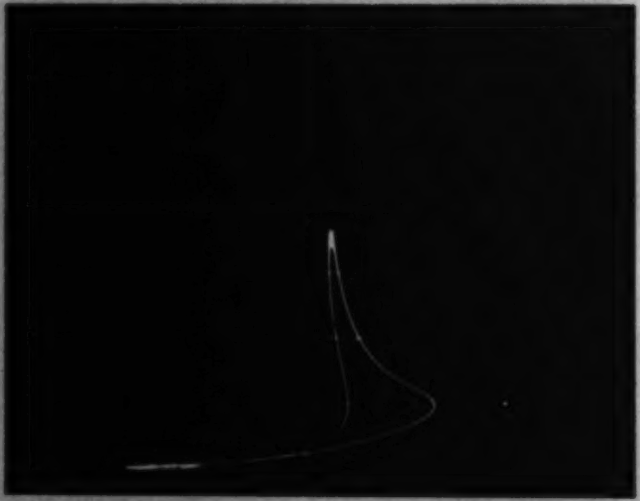

Fig. 35. Oscillograms of the I-V characteristics of oxidized sample SD-4 at (a) 185°K and (b) 183°K. Scales for both oscillograms:

horizontal axis 50 volts/cm
vertical axis 2 mA/cm

(a)

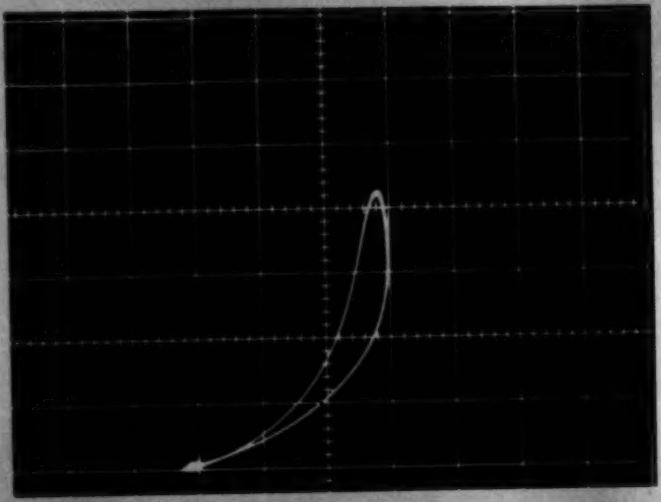

(b)

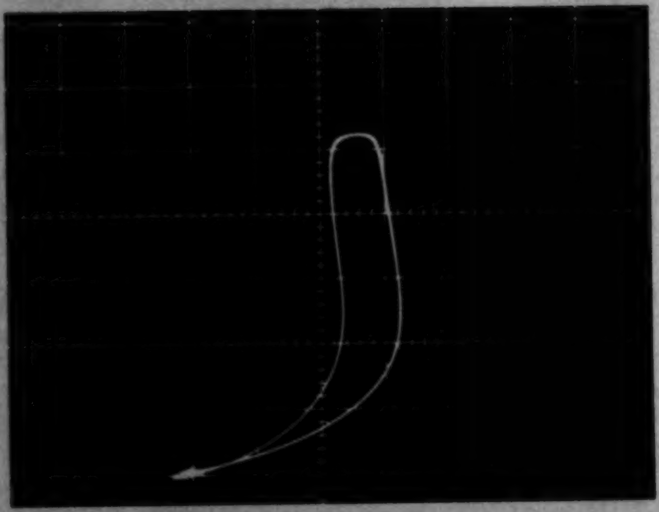

Fig. 36. Oscillogram of the I-V characteristic of oxidized sample SD-4 at 236°K.

Scale: horizontal axis 50 volts/cm
vertical axis 2 mA/cm

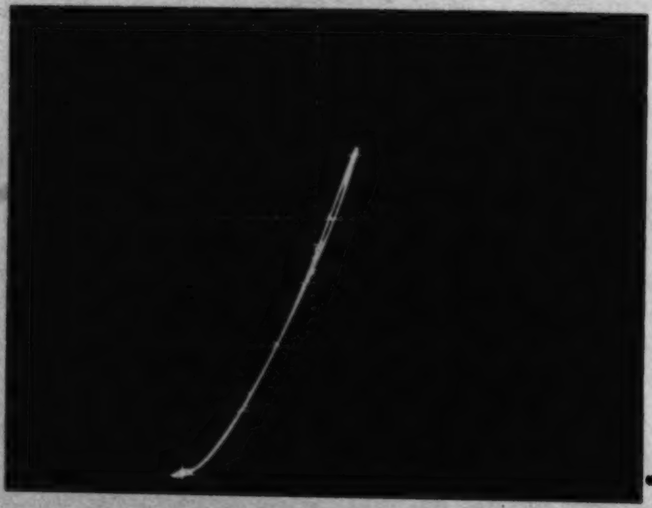

(6) Conclusion for chapter 5:

In this chapter, we have shown that various experimental results indicate that the oxidized samples are double injection diodes, in contrast to that of vacuum-annealed samples. Heating in high oxygen pressure and high temperatures not only increases the low-voltage ohmic resistance, but also affects the Cu-Cu_2O junction, most likely due to the diffusion of oxygen through the boundary.

The simplified theory of double injection with the presence of single-level recombination centers, can account for the low injection level I-V characteristics of thick samples, but discrepencies are observed in thinner samples, as diffusion is expected to be important in these samples.

Preliminary results on negative resistance of oxidized samples are also shown for various temperatures.

Chapter 6

Conclusion

As mentioned in the introductory chapter of this thesis, the original aim of fabricating Cu_2O single crystal diodes was to obtain a better rectifying performance over the conventional Cu_2O multicrystalline diodes. This was not very successful as we reported in chapter 3. However, the results of the behaviour of the single crystal diodes under reversed biased condition does support the suggestion made previously by Weichman and Kuzel (1970a).

Our major aim, however, was shifted as the project progressed. The power relations shown in the forward I-V characteristics caught our attention and our efforts were focussed on investigating these characteristics.

The vacuum-annealed samples, which we have discussed in detail in chapter 4, have shown the various characteristics of that of single injection diodes. The results indicate that there is a continuous distribution of localized states inside these vacuum-annealed samples.

On the other hand, the oxidized samples showed characteristics of double injection diodes (chapter 5). The Cu-Cu_2O junction appears to be affected by the oxidation process and becomes more efficient in injecting electrons. The Ashley-Milnes regimes predicted by the simplified theory of double injection have been observed at low injection level. For thinner samples, however, discrepencies were found. At lower temperatures, negative resistance phenomenon were observed as reported in the end of chapter 5.

To be investigated in further detail remain the physical origin of the continuous localized states, which have also been postulated by Noguet et. al. (1974) in explaining the wide variation of activation energies of Cu_2O crystals. The negative resistance phenomenon observed in the oxidized samples were observed during the final stage of the project when the thesis was being prepared. As a result, only preliminary results could be included as one more piece of experimental evidence for double injection. Remaining to be studied are the post-breakdown regimes where other phenomenon, such as electroluminescence, might be observed.

BIBLIOGRAPHY

Ashley, K.L. and Milnes, A.G. (1964) J. Appl. Phys. 35, 369.

Barnett, A.M. (1970) "Current Filament Formation", in "Semiconductors and Semimetals", vol. 6, (R.K. Willardson and A. Beer, eds., Academic Press, New York.)

Baron, R., Marsh, O.J., and Mayer, J.W. (1966) J. Appl. Phys. 37, 2614.

Baron, R. and Mayer, J.W. (1970) "Double Injection in Semiconductors", in "Semiconductors and Semimetals", vol. 6, (R.K. Willardson and A. Beer, eds., Academic Press, New York.)

Blakemore, J.S. (1962) "Semiconductor Statistics" (Pergamon Press, Oxford.)

Bloem, J. (1958) Philips Res. Repts. 13, 167.

Dean, R.H. (1968) Appl. Phys. Letters, 13, 164.

Dean, R.H. (1969) J. Appl. Phys. 40, 585, 596.

Fortin, E. and Weichman, F.L. (1966) Can. J. Phys. 44, 1551.

Greiner, R.A. (1961) "Semiconductor Devices and Applications" (Mcgraw-Hill, New York.)

Grondahl, L.O. (1933) Rev. Mod. Phys. 5, 141.

Grondahl, L.O. (1926) Phys. Rev. 27, 813.

Kuzel, R. (1961) Direct Current 6, 172.

Kuzel, R., Cann, C.D., Sheinin, S.S. and Weichman, F.L. (1970), Can. J. Phys. 48, 2657.

Kuzel, R. and Weichman, F.L. (1970) J. Appl. Phys. 41, 271.

Lampert, M.A. (1956) Phys. Rev. 103, 1648.

Lampert, M.A. (1959) RCA Rev. 20, 682.

Lampert, M.A. (1962) Phys. Rev. 125, 126.

Lampert, M.A. and Mark, P. (1970) "Current Injection in Solids" (Academic Press, New York).

Lampert, M.A. and Rose, A. (1961) Phys. Rev. 121, 26.

Lanyon, H.P.D. (1963) Phys. Rev. 130, 134.

Lemke, H. (1966) Phys. Status Solidi 16, 413.

Lemke, H. and Muller, G.O. (1967) Phys. Status Solidi 24, 127.

Mark, P. and Helfrich, W. (1962) J. Appl. Phys. 33, 205.

Marsh, D.J. and Viswanathan, C.R. (1967) J. Appl. Phys. 38, 3135.

Mott, N.F. and Gurney, R.W. (1940) "Electronic Processes in Ionic Crystals" (Oxford Univ. Press, London).

Noguet, C., Tapiero, M. and Zielinger, J.P. (1974) Phys. Status Solidi (a), 24, 565.

Pankove, J.I. (1971) "Optical Processes in Semiconductors" (Prentice-Hall, Inc., New Jersey.)

Ridley, B.K. (1963) Proc. Phys. Soc. (London) 82, 954.

Rencroft, P.J. and Mullins, F.D. (1974) J. Phys. Chem. Solids, 35, 347.

Roberts, G.G. (1971) J. Phys. C. : Solid St. Phys. 4, 3167.

Roberts, G.G. and Schmidlin, F.W. (1969) Phys. Rev. 180, 785.

Rose, A. (1955) Phys. Rev. 97, 1538.

Rose, A. (1963) "Concepts in Photoconductivity and Allied Problems" (Interscience Publishers, John Wiley and Sons, New York).

Smith, R.W. (1955) Phys. Rev. 97, 1525.

Tapiero, M., Zielinger, J.P. and Noguet, C. (1976) Phys. Status Solidi (a), 33, 155.

Toth, R.S., Kilkson, R. and Trivich, D. (1961) Phys. Rev. 122, 482.

Tredgold, R.H. (1966) "Space Charge Conduction in Solids" (Elsevier Publishing Company, Amsterdam.)

Weichman, F.L. and Kuzel, R. (1970a) J. Appl. Phys. 41, 3491.

Weichman, F.L. and Kuzel, R. (1970b) Can. J. Phys. 48, 63.

Zielinger, J.P., Tapiero, M. and Noguet, C. (1972) Ann. Phys. 7, 95.

Zouaghi, M., Tapiero, M., Zielinger, J.P. and Burgraf, R. (1970) Solid State Communications, 8, 1823.

Appendix A

List of Symbols

a	ratio μ_p/μ_n
A	area of the injecting contact
$<c_n>$	capture coefficient for electrons
$<c_p>$	capture coefficient for holes
C	capacitance of the sample
D	diffusion coefficient
e	electronic charge
E_a	activation energy
E_F	quasi-Fermi level
$E_{F,o}$	Fermi level at thermal equilibrium
E_o	energy of the lowest-energy hole traps in the trap distribution
E_R	energy of recombination states
E_t	energy of trapping levels
E_v	energy of the valence band edge
g	degeneracy factor
g_h	rate of hole emission from the localized states
$g_{h,o}$	rate of hole emission from the localized states at thermal equilibrium
I	current
I_R	current through the current measuring device

I_s	surface current between the guard ring and the central electrode
J	total current density
J_n	electron current density
J_p	hole current density
k	Boltzmann's constant
ℓ	ratio T_c/T
L	sample thickness
m	electron mass
n	total electron density ($n = n_o + \delta n$)
n_o	thermal equilibrium electron density
n_1	defined as $n_1 = n_o \exp (\frac{E_R - E_F}{kT})$
n_R	electron density on recombination centers
$n_{R,o}$	electron density on recombination centers at thermal equilibrium
δn	excess injected electron density
δn_R	change in the density of electrons occupying recombination centers from thermal equilibrium
N_R	density of recombination centers
N_t	density of traps
N_v	density of states at the valence band edge
p	total hole density ($p = p_o + \delta p$)
p_o	thermal equilibrium hole density
p_1	defined as $p_1 = n_o \exp (\frac{E_R - E_F}{kT})$

$\bar{p}_i$	average injected hole density
$p_{R,o}$	hole density on the recombination centers at thermal equilibrium
p_t	density of trapped holes
δp	excess injected hole density
δp_R	change in the density of holes occupying recombination centers from thermal equilibrium
Q_i	total injected charge
r	rate of recombination
r_h	rate of capturing holes
$r_{h,o}$	rate of capturing holes at thermal equilibrium
r_n	rate of capturing electrons
$r_{n,o}$	rate of capturing electrons at thermal equilibrium
R	internal resistance of the current measuring device
R_s	surface resistance between the guard ring and the central electrode
t_h	average time needed for a hole to escape from a center
t_{ohm}	ohmic relaxation time
T	lattice temperature
T_c	characteristic constant of the trap distribution
v	velocity
V	applied voltage
V_t	transition voltage between the ohmic regime and the SCL conduction regime
x	distance from the anode inside the crystal

μ_n	electron mobility
μ_p	hole mobility
ρ	sample resistivity
σ_n	capture cross section for electrons
σ_p	capture cross section for holes
τ_n	average lifetime for a free electron
τ_h	average lifetime for a free hole
$\tau_{n,o}$	average lifetime for a free electron at thermal equilibrium
$\tau_{p,o}$	average lifetime for a free hole at thermal equilibrium

Appendix B

Recombination Through a Set of Localized States

Recombination of holes and electrons can take place directly from band to band. However, for semiconductors or insulators with a large band gap, recombination of holes and electrons through some localized states inside the band gap is often the dominating recombination mechanism. This involves the successive capture of an electron and hole by a localized trapping state.

The purpose of this short appendix is to derive a relation between the recombination rate, r, and the various quantities such as the densities of free carriers and densities of occupation of the localized states.

Let us consider the case shown in Fig. 24 where the monovalent localized states, at energy E_R, acting as recombination centers, are acceptor-like. In other words, the states are negatively charged when occupied by an electron and neutral when empty. Because of Coulomb attraction, the capture cross-section for holes by an occupied center will be larger than the capture cross-section for electrons for an empty one, that is, $\sigma_p > \sigma_n$.

Let N_R be the total density of the localized recombination states, p, n the densities of free holes and electrons respectively, n_R the density of localized states filled with electrons, p_R the density of localized states which are empty.

It is intuitively clear that the rate of capturing holes, r_h, should be proportional to the density of free holes, p, and also to the density of charged centers, n_R. A more precise form of r_h is given by (refer to, for example, Blakemore 1962),

$$r_h = p < c_p > n_R \tag{B-1}$$

where $<c_p>$, $<c_n>$ are the mean capture coefficients for holes and electrons respectively.

Defining the quantity $\tau_h \equiv \frac{1}{n_R<c_p>}$, which is known as the average lifetime for a free hole, the rate of capturing holes can also be written as,

$$r_h = \frac{p}{\tau_h}$$

Since the holes can also escape from the localized states, the net rate of capturing holes by the localized states is given by,

$$r = r_h - g_h \tag{B-2}$$

where g_h is the rate of hole emission from the empty localized states.

The rates of the emission of holes at non-equilibrium can be obtained from the rates of emission when the crystal is at equilibrium.

At thermal equilibrium, the capture of holes on the localized states must be balanced by the reverse process of emission of holes. Thus we have,

$$r_{h,o} = g_{h,o} \tag{B-3}$$

where the subscript o denotes thermal equilibrium condition.

Thus, since

$$r_{h,o} = \frac{p_o}{\tau_{h,o}}$$

and

$$g_{h,o} = \frac{p_{R,o}}{t_h} ,$$

we have,

$$\frac{p_o}{\tau_{h,o}} = \frac{p_{R,o}}{t_h}$$

where t_h is the average time needed for a hole to escape from a center, leaving it negatively charged, and $\tau_{h,o}$ the average lifetime of free holes at thermal equilibrium.

Thus,

$$t_h = \tau_{h,o} \frac{p_{R,o}}{p_o}$$

or,

$$t_h = \frac{p_{R,o}}{\langle c_p \rangle n_{R,o} p_o} \tag{B-4}$$

since

$$\tau_{h,o} = \frac{1}{\langle c_p \rangle n_{R,o}} .$$

The rate of hole emission from the centers under injection condition is then given by,

$$g_h = \frac{p_R}{t_h} = \frac{p_R}{p_{R,o}} <c_p> n_{R,o}\, P_o \qquad \text{(B-5)}$$

From (B-1), (B-2) and (B-5), we have,

$$r = p<c_p>n_R - P_R<c_p> \frac{n_{R,o}}{p_{R,o}}\; P_o \qquad \text{(B-6)}$$

Let P_o be the density of free holes at thermal equilibrium, and δp the density of excess free holes under injection condition, we have,

$$p = p_o + \delta p \qquad \text{(B-7)}$$

Also, let δn_R be the change in the density of localized states filled by electrons under injection condition, and δp_R the change in the density of empty centers under injection condition. We have,

$$\begin{aligned} p_R &= p_{R,o} + \delta p_R \\ n_R &= n_{R,o} + \delta n_R \end{aligned} \qquad \text{(B-8)}$$

To write (B-6) in terms of the quantities δp, δp_R, δn_R, we note that,

$$n_{R,o} = \frac{N_R}{1 + \exp \frac{(E_R - E_F)}{kT}} \qquad \text{(B-9)}$$

and,

$$p_{R,o} = [1 - \frac{1}{1 + \exp(\frac{E_R - E_F}{kT})}] N_R \qquad \text{(B-10)}$$

where E_F is the Fermi level at thermal equilibrium.

Introducing quantities n_1, p_1, which are defined as,

$$n_1 = N_c \exp(\frac{E_R - E_C}{kT}) = n_o \exp(\frac{E_R - E_F}{kT}), \qquad \text{(B-11)}$$

$$p_1 = N_V \exp(\frac{E_V - E_R}{kT}) = p_o \exp(\frac{E_F - E_R}{kT}), \qquad \text{(B-12)}$$

From (B-11), (B-12), we have,

$$\frac{n_1}{n_o} = \frac{p_o}{p_1}$$

We have from (B-6) and (B-7),

$$p_{R,o} = N_R [1 - \frac{1}{1 + \frac{p_o}{p_1}}]$$

$$= N_R \frac{p_o}{p_1 + p_o} \qquad \text{(B-13)}$$

$$n_{R,o} = N_R \frac{1}{1 + \frac{n_1}{n_o}}$$

$$= N_R \frac{p_1}{p_1 + p_o} \qquad \text{(B-14)}$$

$$\frac{n_{R,o}}{p_{R,o}} = \frac{p_1}{p_o} \qquad \text{(B-15)}$$

From (B-5), we have,

$$g_h = p_R\, p_o \,\langle c_p\rangle \left(\frac{p_1}{p_o}\right)$$

$$= p_R \,\langle c_p\rangle\, p_1 \qquad \text{(B-16)}$$

Thus, from (B-6),

$$r = p\langle c_p\rangle n_R - p_R\langle c_p\rangle p_1$$

$$= [(p_o+\delta p)(n_{R,o}+\delta n_R) - (p_{R,o}+\delta p_R)p_1]\langle c_p\rangle$$

$$= [\delta p\; n_{R,o} + (p_o+\delta p+p_1)\cdot\delta n_R]\langle c_p\rangle \qquad \text{(B-17)}$$

since $\delta p_R = -\delta n_R$ (because $p_R + n_R = N_R$).

Similarly, we get,

$$r = [\delta n\; p_{R,o} - (n_o+\delta n+n_1)\cdot\delta n_R]\langle c_n\rangle \qquad \text{(B-18)}$$